J. Appl. Comput. Mech., 5(1) (2019) 13-39
DOI: 10.22055/JACM.2018.24529.1196

ISSN: 2383-4536
jacm.scu.ac.ir

M&MoCS
Shahid Chamran University of Ahvaz

Journal of Applied and Computational Mechanics

Research Paper

Free Convection Flow and Heat Transfer of Nanofluids of Different Shapes of Nano-Sized Particles over a Vertical Plate at Low and High Prandtl Numbers

M.G. Sobamowo

Department of Mechanical Engineering, University of Lagos, Akoka, Lagos, Nigeria.

Received December 28 2017; Revised January 29 2018; Accepted for publication March 20 2018.
Corresponding author: M.G. Sobamowo, mikegbeminiyi@gmail.com

Abstract. In this paper, free convection flow and heat transfer of nanofluids of differently-shaped nano-sized particles over a vertical plate at very low and high Prandtl numbers are analyzed. The governing systems of nonlinear partial differential equations of the flow and heat transfer processes are converted to systems of nonlinear ordinary differential equation through similarity transformations. The resulting systems of fully-coupled nonlinear ordinary differential equations are solved using a differential transformation method - Padé approximant technique. The accuracy of the developed approximate analytical methods is verified by comparing the results of the differential transformation method - Padé approximant technique with those of previous works as presented in the literature. Thereafter, the analytical solutions are used to investigate the effects of the Prandtl number, the nanoparticles volume-fraction, the shape and the type on the flow and heat transfer behaviour of various nanofluids over the flat plate. It is observed that as the Prandtl number and volume-fraction of the nanoparticles in the basefluid increase, the velocity of the nanofluid decreases while the temperature increases. Also, the maximum decrease in velocity and the maximum increase in temperature are recorded in lamina-shaped nanoparticles, followed by platelets, cylinders, bricks, and sphere-shaped nanoparticles, respectively. Using a common basefluid for all nanoparticle types, it is established that the maximum decrease in velocity and the maximum increase in temperature are recorded in TiO2 followed by CuO, Al_2O_3 and SWCNTs nanoparticles, respectively. It is hoped that the present study will enhance the understanding of free convection boundary-layer problems as applied in various industrial, biological and engineering processes.

Keywords: Free convection; Boundary layer; Prandtl number; Nanofluid; Differential transformation method; Padé-approximant technique.

1. Introduction

The importance and the wide applications of free convection flow and heat transfer in extrusion, melt spinning, glass-fibre production processes, food processing, mechanical forming processes, etc. have recently aroused renewed research interests and explorations in fluid dynamics studies. In the study of free convection and heat transfer problems, the analysis of incompressible laminar flow of viscous fluid in a steady state, two-dimensional free-convection boundary-layer has over the years been a common area of increasing research interests following the experimental investigations of Schmidt and Beckmann [1] and the pioneering theoretical work of Ostrach et al. [2]. In their attempt to study the laminar free convection flow and heat transfer problem in 1953, Ostrach et al. [2] applied the method of iterative integration to analyze free-convection over a semi-infinite isothermal flat plate. The authors obtained numerical solutions for a wide range of Prandtl numbers from 0.01 to 1000 and validated their numerical results using experimental data of Schmidt and Beckmann [1]. Five years later, Sparrow and

Published online December 11 2018

Gregg [3] presented a further study on numerical solutions for laminar free convection over a vertical plate with uniform surface heat flux. Considering the fact that the major part of low Prandtl number boundary layer of free convection is inviscid, Lefevre [4] examined the laminar free convection of an inviscid flow from a vertical plane surface. In a further work, Sparrow and Gregg [5] developed similar solutions for free convection from a non-isothermal vertical plate. Meanwhile, a study on fluid flow over a heated vertical plate at high Prandtl numbers was presented by Stewartson and Jones [6]. Due to the disadvantages in the numerical methods in the previous studies [2, 3], Kuiken [7] adopted the method of matched asymptotic expansion and established asymptotic solutions for large Prandtl number free-convection. In the subsequent year, the same author applied the singular perturbation method and analyzed free-convection at low Prandtl numbers [8]. Also, in another work on the asymptotic analysis of the same problem, Eshghy [9] studied free convection boundary layers at large Prandtl numbers while Roy [10] investigated free convection for uniform surface heat flux at high Prandtl numbers. With the development of asymptotic solution, a combined study of the effects of small and high Prandtl numbers on the viscous fluid flow over a flat vertical plate was submitted by Kuiken and Rotem [11]. In the succeeding year, Na and Habib [12] applied the parameter differentiation method to solve the free-convection boundary layer problem. Few years later, Merkin [13] presented the similarity solutions for free-convection on a vertical plate while Merkin and Pop [14] used the finite difference method to develop numerical solutions for conjugate free convection problem of boundary layer flow over a vertical plate. Also, Ali et al. [15] submitted a study on numerical investigation of free-convective boundary layer in a viscous fluid.

The various analytical and numerical studies of the past works have shown that the boundary layer problems are very difficult to solve. This is because, besides having very thin regions where there is a rapid change of the fluid properties they are defined on unbounded domains. Although different analytical methods have been used to solve boundary layer problems, they converge very slowly for some boundary layer problems, particularly for those with very large parameters. The numerical methods applied to the flow process also encounter some problems in resolving the solution of the governing equations in very thin regions and in cases where singularities or multiple solutions exist. Moreover, in numerical analysis, it is absolutely required that the stability and convergence analysis should be carried out so as to avoid divergence or inappropriate results. It is such an exercise in the mathematical methods that increases the computation time and the cost of numerical methods. Therefore, in the quest of presenting symbolic solutions to the flow and heat transfer problem using one of the recently developed semi-analytical methods, Motsa et al. [16] adopted homotopy analysis of free-convection boundary layer flow with heat and mass transfer. In another work, the authors used spectral local linearization approach for solving the natural convection boundary layer flow [17]. With an extended interest on the flow problem, Ghotbi et al. [18] investigated the application of the homotopy analysis method to natural convection boundary layer flow. Although the homotopy analysis method (HAM) is a reliable and efficient semi-analytical technique, it suffers from a number of limiting assumptions such as the requirements that the solution ought to conform to the so-called rule of solution expression and the rule of coefficient ergodicity. Moreover, the use of HAM in the analysis of linear and nonlinear equations requires the determination of auxiliary parameters which increase the computational cost and time. Additionally, the lack of rigorous theories or proper guidance for choosing initial approximation, auxiliary linear operators, auxiliary functions, and auxiliary parameters limits the applications of HAM. In addition, such a method requires high skills in mathematical analysis and its solution comes with a large number of terms. Additionally, various analyses of nonlinear models and fluid flow problems under the influences of some internal and external factors using different approximate analytical and numerical methods have been presented in the literature [19-39]. However, the relative simplicity coupled with the ease of applications of differential transformation method (DTM) has shown that the method is more effective in principle and application than most of the other approximate analytical methods. The differential transformation method, as introduced by Zhou [40], has fast gained ground as it has appeared in many engineering and scientific research papers. This is because, with the applications of DTM, a closed form series solution or approximate solution can be provided for nonlinear integral and differential equations without linearization, restrictive assumptions, perturbation and discretization or round-off error. The method reduces the complexity of the expansion of derivatives and the computational difficulties of the other traditional or recently-developed methods. Therefore, Yu and Chen [41] applied the differential transformation method to provide approximate analytical solutions to the Blasius equation. Also, Kuo [42] adopted the same method to determine the velocity and temperature profiles of the Blasius equation of forced convection problem for fluid flow passing over a flat plate. A further work on the applications of differential transformation method to free convection boundary-layer problem of two-dimensional steady and incompressible laminar flow passing over a vertical plate was presented by the same author [43]. However, in the later work, the nonlinear coupled boundary value governing equations of the flow and heat transfer processes were reduced to initial value equations by a group of transformations and the resulting coupled initial-value equations were solved by means of the differential transformation method. The reduction or the transformation of the boundary value problems to the initial value problems was carried out due to the fact that the developed systems of nonlinear differential equations contain an unbounded domain of infinite boundary conditions. Moreover, in order to obtain the numerical solutions that are valid over the entire large domain of the problem, Ostrach et al. [2] estimated the values of an unknown boundary condition in the analysis of the developed systems of fully coupled nonlinear ordinary differential equations. Following the Ostrach et al.'s approach, most of the subsequent solutions provided in the literature [3, 9, 10, 12, 14, 15, 42, and 43] were based on the estimated boundary conditions given by Ostrach et al. [1]. Additionally, the limitations of power series solutions to small domain problems have been well established in literature. However, in some recent studies, the use of power series methods coupled with the Padé-approximant technique has been found to be a very effective way of developing accurate analytical solutions to nonlinear problems of large or unbounded domain problems of infinite boundary conditions. The application of the Padé-approximant technique with power series method increases the rate of convergence and the radius of convergence of power series solution. Therefore, in a recent work, Rashidi et al. [44] applied the differential transformation method coupled with the Padé-approximant technique to develop a novel analytical solution for mixed convection about an inclined flat plate embedded in a porous medium.

The previous studies on the problem under investigation are based on viscous fluid flow as shown in the works reviewed above. To the best of the author's knowledge, a study on the influence of nanoparticle shape, size and type on the free convection boundary layer flow and heat transfer of nanofluids over a vertical plate at low and high Prandtl numbers using the differential transformation method coupled with the Padé-approximant technique has not been presented in literature. Therefore, the present study focuses on the application of the differential transformation method coupled with the Padé-approximant technique to develop approximate analytical solutions and carry out parametric studies for the free convection boundary-layer flow and heat transfer of nanofluids of different shapes nano-sized particles over a vertical plate at low and high Prandtl numbers. Another novelty of the present study is the development of approximate analytical solutions for the free convection boundary layer problem without using the estimated boundary conditions during the analysis of the problem.

2. Problem formulation and mathematical analysis

Consider a laminar free-convection flow of an incompressible nanofluid over a vertical plate parallel to the direction of the generating body force as shown in Fig. 1. Assuming that the flow in the laminar boundary layer is two-dimensional and steady, the physical and thermal properties of the fluid are constant, the equations for continuity and motion are given as

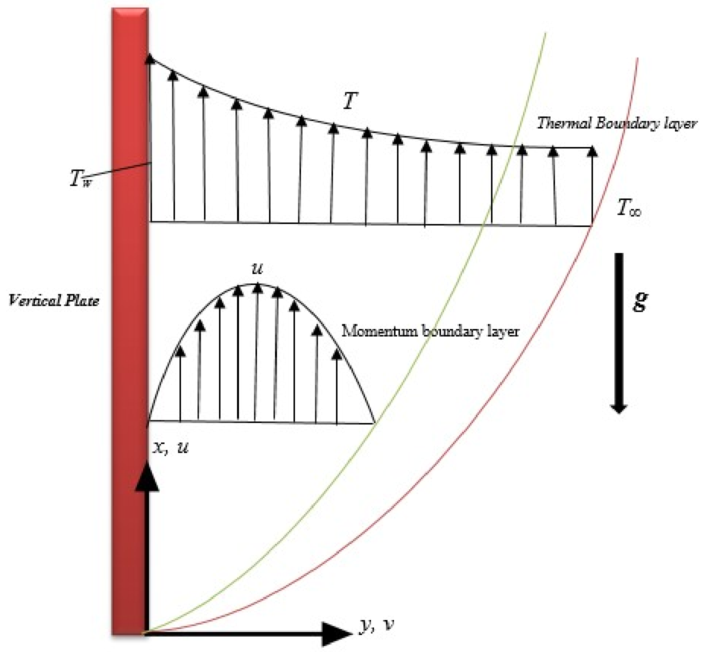

Fig. 1. Velocity and temperature profiles in free-convection flow over a vertical plate

$$\frac{\partial u}{\partial x}+\frac{\partial v}{\partial y}=0 \tag{1}$$

$$\rho_{nf}\left(u\frac{\partial u}{\partial x}+v\frac{\partial u}{\partial y}\right)=\mu_{nf}\frac{\partial^2 u}{\partial y^2}+g\left(\rho\beta\right)_{nf}\left(T-T_\infty\right) \tag{2}$$

$$\left(\rho c_p\right)_{nf}\left(u\frac{\partial T}{\partial x}+v\frac{\partial T}{\partial y}\right)=k_{nf}\frac{\partial^2 T}{\partial y^2} \tag{3}$$

With no-slip conditions, the appropriate boundary conditions are given as

$$u=0,\quad v=0,\quad T=T_s\quad at\quad y=0 \tag{4a}$$

$$u=0,\quad T=T_w,\quad at\ y\to\infty \tag{4b}$$

where the various physical and thermal properties in Eqs. (1-3) are given as

$$\rho_{nf}=\rho_f\left(1-\phi\right)+\rho_s\phi \tag{5a}$$

$$\left(\rho c_p\right)_{nf}=\left(\rho c_p\right)_f\left(1-\phi\right)+\left(\rho c_p\right)_s\phi \tag{5b}$$

$$\left(\rho\beta\right)_{nf}=\left(\rho\beta\right)_f\left(1-\phi\right)+\left(\rho\beta\right)_s\phi \tag{5c}$$

$$\mu_{nf} = \frac{\mu_f}{(1-\phi)^{2.5}} \tag{5d}$$

$$k_{nf} = k_f \left[\frac{k_s + (m-1)k_f - (m-1)\phi(k_f - k_s)}{k_s + (m-1)k_f + \phi(k_f - k_s)} \right] \tag{6}$$

where m in the above Hamilton Crosser's model in Eq. (6) is the shape factor for which the numerical values for different shapes are given in Table 1. It should be noted that in the shape factor, $m = 3/\lambda$, λ is the sphericity (the ratio of the surface area of the sphere and the surface area of the real particles with equal volumes). For sphericity of sphere, platelet, cylinder, laminar and brick, the values are *1.000, 0.526, 0.625, 0.185* and *0.811*, respectively. The Hamilton Crosser's model becomes a Maxwell-Garnett's model when the shape factor of the nanoparticle is $m=3$.

Table 1. The values of different shapes of nanoparticles [45, 46]

S/N	Name	Shape	Shape factor (m)	Sphericity(ψ)
1	Sphere	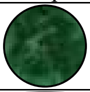	3.0	1.000
2	Platelet		5.7	0.526
3	Cylinder	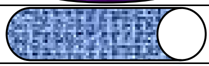	4.8	0.625
4	Lamina		16.2	0.185
5	Brick	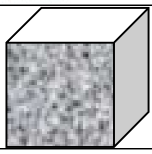	3.7	0.811

Table 2 and 3 present the physical and thermal properties of the base fluid and the nanoparticles, respectively. SWCNTs mean single-walled carbon nanotubes.

Table 2. Physical and thermal properties of the base fluid [45-50]

Base fluid	ρ (kg/m^3)	c_p (J/kgK)	k (W/mK)
Pure water	997.1	4179	0.613
Ethylene Glycol	1115	2430	0.253
Engine oil	884	1910	0.144
Kerosene	783	2010	0.145

Table 3. Physical and thermal properties of nanoparticles [45-50]

Nanoparticles	ρ (kg/m^3)	c_p (J/kgK)	k (W/mK)
Copper (Cu)	8933	385	401
Aluminum oxide (Al2O3)	3970	765	40
SWCNTs	2600	42.5	6600
Silver (Ag)	10500	235.0	429
Titanium dioxide (TiO2)	4250	686.2	8.9538
Copper (II) Oxide (CuO)	783	540	18

Going back to Eqs. (1), (2) and (3) and if one introduces a stream function, $\psi(x, y)$ such that

$$u = \frac{\partial \psi}{\partial y}, \quad v = -\frac{\partial \psi}{\partial x}, \tag{7}$$

and use the following similarity and dimensionless variables

$$\eta=\left[\frac{\rho_f^2\left(g\beta_f\left(T_w-T_\infty\right)\right)}{4\mu_f^2 x}\right]^{\frac{1}{4}} y,\qquad \psi=\frac{4\mu_f}{\rho_f}\left[\frac{\rho_f^2\left(g\beta_f\left(T_w-T_\infty\right)\right)x^3}{4\mu_f^2}\right]^{1/4} f(\eta),\qquad \theta=\frac{T-T_\infty}{T_w-T_\infty}, Pr=\frac{\mu_f c_p}{k_f}, \tag{8}$$

one arrives at fully coupled third- and second-order ordinary differential equations

$$f'''+(1-\phi)^{2.5}\left\{\left[(1-\phi)+\phi\left(\frac{\rho_s}{\rho_f}\right)\right]\left(3ff''-2(f')^2\right)+\left[(1-\phi)+\phi\left[(\rho\beta)_s/(\rho\beta)_f\right]\right]\theta\right\}=0 \tag{9}$$

$$\theta''+3\left[\frac{1}{\left[(1-\phi)+\phi\left[(\rho C_p)_s/(\rho C_p)_f\right]\right]}\left[\frac{k_s+(m-1)k_f-(m-1)\phi(k_f-k_s)}{k_s+(m-1)k_f+\phi(k_f-k_s)}\right]\right]Prf\,\theta'=0 \tag{10}$$

and the boundary conditions as

$$\begin{aligned} &f=0,\quad f'=0,\quad \theta=1,\quad when\ \ \eta=0\\ &f'=0,\quad \theta=0,\quad when\ \ \eta=\infty \end{aligned} \tag{11}$$

The procedures of the transformation of the nonlinear partial differential equations (1-3) to the nonlinear ordinary differential equations (9-10) with their corresponding boundary conditions are shown in the Appendix A.

It should be noted that for a viscous fluid which does not have nanoparticles, the nanoparticle volume fraction is zero, i.e. $\phi=0$ and then one recovers the earlier models [2-15] from Eqs. (9) and (10), which are

$$f'''+3ff''-2(f')^2+\theta=0 \tag{12}$$

$$\theta''+3Prf\,\theta'=0 \tag{13}$$

and the boundary conditions remain the same as in Eq. (11)

3. Method of solution: Differential transform method

The relatively new semi-analytical method, the differential transformation method introduced by Zhou [40], has proved very effective in providing highly accurate solutions to differential equations, difference equation, differential-difference equations, fractional differential equation, pantograph equation and integro-differential equation. Therefore, this method was applied to the present study. The basic definitions and the operational properties of the method are as follows:

If $u(t)$ is analytic in the domain T, then the function $u(t)$ will be differentiated continuously with respect to time *t.*

$$\frac{d^p u(t)}{dt^p}=\varphi(t,p)\qquad \text{for all}\qquad t\in T \tag{14}$$

for $t=t_i$, then $\varphi(t,p)=\varphi(t_i,p)$, where *p* belongs to the set of non-negative integers, denoted as the *p*-domain. We can therefore write Eq. (14) as

$$U(p)=\varphi(t_i,p)=\left[\frac{d^p u(t)}{dt^p}\right]_{t=t_i} \tag{15}$$

where U_p is called the spectrum of $u(t)$ at $t=t_i$. Expressing $u(t)$ in Taylor's series as

$$u(t)=\sum_{p}^{\infty}\left[\frac{(t-t_i)^p}{p!}\right]U(p) \tag{16}$$

where Eq. (14) is the inverse of $U(k)$ us symbol 'D' denoting the differential transformation process and combining (15) and (16), we have

$$u(t)=\sum_{p=0}^{\infty}\left[\frac{(t-t_i)^p}{p!}\right]U(p)=D^{-1}U(p) \tag{17}$$

Using the operational properties of the differential transformation method from Table 4, the differential transformation of the governing differential Eq. (9) is given as

$$(p+1)(p+2)(p+3)F(p+3)+(1-\phi)^{2.5}\left\{\begin{aligned}&\left[(1-\phi)+\phi\left(\frac{\rho_s}{\rho_f}\right)\right]\left[\begin{aligned}&3\sum_{l=0}^{p}(p-l+1)(p-l+2)F(l)F(p-l+2)\\&-2\sum_{l=0}^{p}(l+1)(p-l+1)F(l+1)F(p-l+1)\end{aligned}\right]\\&+\left[(1-\phi)+\phi\left[(\rho\beta)_s/(\rho\beta)_f\right]\right]\Theta(p)\end{aligned}\right\}=0 \tag{18}$$

Table 4. Operational properties of differential transformation method

S/N	Function	Differential transform
1	$u(t)\pm v(t)$	$U(p)\pm V(p)$
2	$\alpha u(t)$	$\alpha U(p)$
3	$\frac{du(t)}{dt}$	$(p+1)\,U(p+1)$
4	$u(t)v(t)$	$\sum_{r=0}^{p} V(r)U(p-r)$
5	$u^m(t)$	$\sum_{r=0}^{p} U^{m-1}(r)U(p-r)$
6	$\frac{d^n u(t)}{dx^n}$	$(p+1)(p+2)\text{L}\ (p+n)U(p+n)$
7	$\sin(\omega t+\alpha)$	$\frac{\omega^p}{\text{p}!}\sin\left(\frac{\pi p}{2!}+\alpha\right)$
8	$\cos(\omega t+\alpha)$	$Z(p)=\frac{\omega^p}{\text{p}!}\cos\left(\frac{\pi p}{2!}+\alpha\right)$

Equivalently, we can write the recursive relation for Eq. (18) in DTM domain as

$$F(p+3)=\frac{(1-\phi)^{2.5}}{(p+1)(p+2)(p+3)}\left\{\begin{array}{l}\left[(1-\phi)+\phi\left(\frac{\rho_s}{\rho_f}\right)\right]\left[\begin{array}{l}2\sum_{l=0}^{p}(l+1)(p-l+1)F(l+1)F(p-l+1)\\-3\sum_{l=0}^{p}(p-l+1)(p-l+2)F(l)F(p-l+2)\end{array}\right]\\-\left[(1-\phi)+\phi\left[(\rho\beta)_s/(\rho\beta)_f\right]\right]\Theta(p)\end{array}\right\} \tag{19}$$

For Eq.(10), we have the recursive relation in the differential transform domain as

$$(p+1)(p+2)\Theta(p+2)+\left\{\begin{array}{l}3Pr\left[\frac{1}{\left[(1-\phi)+\phi\left[(\rho C_p)_s/(\rho C_p)_f\right]\right]}\left[\frac{k_s+(m-1)k_f-(m-1)\phi(k_f-k_s)}{k_s+(m-1)k_f+\phi(k_f-k_s)}\right]\right]\\\times\sum_{l=0}^{p}(l+1)\Theta(l+1)F(p-l)\end{array}\right\}=0 \tag{20}$$

which can be written as

$$\Theta(p+2)=\frac{-3Pr}{(p+1)(p+2)}\left\{\begin{array}{l}\left[\frac{1}{\left[(1-\phi)+\phi\left[(\rho C_p)_s/(\rho C_p)_f\right]\right]}\left[\frac{k_s+(m-1)k_f-(m-1)\phi(k_f-k_s)}{k_s+(m-1)k_f+\phi(k_f-k_s)}\right]\right]\\\times\sum_{l=0}^{p}(l+1)\Theta(l+1)F(p-l)\end{array}\right\} \tag{21}$$

Also, the recursive relations for the boundary conditions in Eq.(12) are

$$\begin{array}{l}F(p)=0\Rightarrow F(0)=0,\quad (p+1)F(p+1)=0\quad\Rightarrow F(1)=0,\quad \theta(p)=1\quad\Rightarrow\theta(0)=1,\\F(2)=\frac{a}{2},\quad \theta(1)=b,\end{array} \tag{22}$$

where a and b are unknown constants to be found later. From Eq. (22), we have the following boundary conditions in the differential transform domain

$$F(0)=0,\quad F(1)=0,\quad \theta(0)=1,\quad F(2)=\frac{a}{2},\quad \theta(1)=b \tag{23}$$

Using *p=0, 1, 2, 3, 4, 5, 6, 7…* in the above recursive relations in Eq. (18), we arrived at

$$F[3]=\frac{-(1-\phi)^{2.5}}{6}\left\{(1-\phi)+\phi\left[(\rho\beta)_s/(\rho\beta)_f\right]\right\},\quad F[4]=\frac{-(1-\phi)^{2.5}}{24}\left\{(1-\phi)+\phi\left[(\rho\beta)_s/(\rho\beta)_f\right]\right\}b$$

$$F[5]=\frac{(1-\phi)^{2.5}}{120}\left\{(1-\phi)+\phi\left(\frac{\rho_s}{\rho_f}\right)\right\}a^2,\quad F[6]=0$$

$$F[7]=\frac{(1-\phi)^{2.5}}{210}\left(\begin{array}{l}
2\left\{(1-\phi)+\phi\left(\dfrac{\rho_s}{\rho_f}\right)\right\}\left(\begin{array}{l}-\left(\dfrac{1}{3}\right)(1-\phi)^{2.5}\left\{(1-\phi)+\phi\left[(\rho\beta)_s/(\rho\beta)_f\right]\right\}ab\\ +\left(\dfrac{1}{4}\right)(1-\phi)^{5}\left\{(1-\phi)+\phi\left[(\rho\beta)_s/(\rho\beta)_f\right]\right\}^2\end{array}\right)\\
-3\left\{(1-\phi)+\phi\left(\dfrac{\rho_s}{\rho_f}\right)\right\}\left(\begin{array}{l}\dfrac{-7(1-\phi)^{2.5}}{24}\left\{(1-\phi)+\phi\left[(\rho\beta)_s/(\rho\beta)_f\right]\right\}ab\\ +\dfrac{(1-\phi)^{5}}{6}\left\{(1-\phi)+\phi\left[(\rho\beta)_s/(\rho\beta)_f\right]\right\}^2\end{array}\right)\\
+\dfrac{\left\{(1-\phi)+\phi\left[(\rho\beta)_s/(\rho\beta)_f\right]\right\}Pr}{8}\left\{\begin{array}{l}\dfrac{1}{\left[(1-\phi)+\phi\left[(\rho c_p)_s/(\rho c_p)_f\right]\right]}\cdot\\ \left[\dfrac{k_s+(m-1)k_f-(m-1)\phi(k_f-k_s)}{k_s+(m-1)k_f+\phi(k_f-k_s)}\right]\end{array}\right\}ab
\end{array}\right)$$

$$F[8]=\frac{(1-\phi)^{2.5}}{336}\left(\begin{array}{l}
2\left\{(1-\phi)+\phi\left(\dfrac{\rho_s}{\rho_f}\right)\right\}\left(\begin{array}{l}\dfrac{(1-\phi)^{2.5}}{12}\left\{(1-\phi)+\phi\left(\dfrac{\rho_s}{\rho_f}\right)\right\}a^3\\ +\dfrac{(1-\phi)^{5}}{6}\left\{(1-\phi)+\phi\left[(\rho\beta)_s/(\rho\beta)_f\right]\right\}^2 b\end{array}\right)\\
-3\left\{(1-\phi)+\phi\left(\dfrac{\rho_s}{\rho_f}\right)\right\}\left(\begin{array}{l}\dfrac{11(1-\phi)^{2.5}}{20}\left\{(1-\phi)+\phi\left(\dfrac{\rho_s}{\rho_f}\right)\right\}a^3\\ +\dfrac{(1-\phi)^{5}}{8}\left\{(1-\phi)+\phi\left[(\rho\beta)_s/(\rho\beta)_f\right]\right\}^2 b\end{array}\right)\\
-\left(\dfrac{\left\{(1-\phi)+\phi\left[(\rho\beta)_s/(\rho\beta)_f\right]\right\}^2 Pr(1-\phi)^{2.5}}{40}\right)\left\{\begin{array}{l}\dfrac{1}{\left[(1-\phi)+\phi\left[(\rho c_p)_s/(\rho c_p)_f\right]\right]}\cdot\\ \left[\dfrac{k_s+(m-1)k_f-(m-1)\phi(k_f-k_s)}{k_s+(m-1)k_f+\phi(k_f-k_s)}\right]\end{array}\right\}b
\end{array}\right)$$

$$F[9]=\frac{(1-\phi)^{2.5}}{540}\left(\begin{array}{l}
2\left\{(1-\phi)+\phi\left(\dfrac{\rho_s}{\rho_f}\right)\right\}\left(\begin{array}{l}-\dfrac{(1-\phi)^{5}}{24}\left\{(1-\phi)+\phi\left[(\rho\beta)_s/(\rho\beta)_f\right]\right\}\left\{(1-\phi)+\phi\left(\dfrac{\rho_s}{\rho_f}\right)\right\}a^2\\ +\dfrac{(1-\phi)^{5}}{36}\left\{(1-\phi)+\phi\left[(\rho\beta)_s/(\rho\beta)_f\right]\right\}^2 b^2\end{array}\right)\\
-3\left\{(1-\phi)+\phi\left(\dfrac{\rho_s}{\rho_f}\right)\right\}\left(\begin{array}{l}-\left(\dfrac{13(1-\phi)^{5}}{360}\right)\left\{(1-\phi)+\phi\left[(\rho\beta)_s/(\rho\beta)_f\right]\right\}\left\{(1-\phi)+\phi\left(\dfrac{\rho_s}{\rho_f}\right)\right\}a^2\\ +\left(\dfrac{(1-\phi)^{5}}{48}\right)\left\{(1-\phi)+\phi\left[(\rho\beta)_s/(\rho\beta)_f\right]\right\}^2 b^2\end{array}\right)\\
-\left(\dfrac{\left\{(1-\phi)+\phi\left[(\rho\beta)_s/(\rho\beta)_f\right]\right\}^2}{240}\right)Pr\left\{\begin{array}{l}\dfrac{1}{\left[(1-\phi)+\phi\left[(\rho c_p)_s/(\rho c_p)_f\right]\right]}\cdot\\ \left[\dfrac{k_s+(m-1)k_f-(m-1)\phi(k_f-k_s)}{k_s+(m-1)k_f+\phi(k_f-k_s)}\right]\end{array}\right\}(1-\phi)^{2.5}b^2
\end{array}\right)$$

$$
\begin{aligned}
F[10]=\frac{(1-\phi)^{2.5}}{720}\Bigg\{ & 2\left\{(1-\phi)+\phi\left(\frac{\rho_s}{\rho_f}\right)\right\}\Bigg(\left(\frac{a(1-\phi)^{2.5}}{15}\right)\Bigg[2\left\{(1-\phi)+\phi\left(\frac{\rho_s}{\rho_f}\right)\right\}\left(\begin{aligned}&-\left(\frac{a(1-\phi)^{2.5}}{3}\right)\left\{(1-\phi)+\phi\left[(\rho\beta)_s/(\rho\beta)_f\right]\right\}b\\&+\left(\frac{(1-\phi)^{2.5}}{4}\right)\left\{(1-\phi)+\phi\left[(\rho\beta)_s/(\rho\beta)_f\right]\right\}^2\end{aligned}\right)\\
&-3\left\{(1-\phi)+\phi\left(\frac{\rho_s}{\rho_f}\right)\right\}\left(\begin{aligned}&-\left(\frac{7a(1-\phi)^{2.5}}{24}\right)\left\{(1-\phi)+\phi\left[(\rho\beta)_s/(\rho\beta)_f\right]\right\}b\\&+\left(\frac{(1-\phi)^{5}}{6}\right)\left\{(1-\phi)+\phi\left[(\rho\beta)_s/(\rho\beta)_f\right]\right\}^2\end{aligned}\right)\\
&+\left(\frac{\left\{(1-\phi)+\phi\left[(\rho\beta)_s/(\rho\beta)_f\right]\right\}Pr}{8}\right)\left\{\frac{1}{\left[(1-\phi)+\phi\left[(\rho c_p)_s/(\rho c_p)_f\right]\right]}\cdot\left[\frac{k_s+(m-1)k_f-(m-1)\phi(k_f-k_s)}{k_s+(m-1)k_f+\phi(k_f-k_s)}\right]\right\}ab\Bigg]\\
&-\left(\frac{(1-\phi)^5\left\{(1-\phi)+\phi\left[(\rho\beta)_s/(\rho\beta)_f\right]\right\}}{72}\right)\left\{(1-\phi)+\phi\left(\frac{\rho_s}{\rho_f}\right)\right\}a^2b\Bigg)\\
&-3\left\{(1-\phi)+\phi\left(\frac{\rho_s}{\rho_f}\right)\right\}\Bigg(\left(\frac{11a(1-\phi)^{2.5}}{105}\right)\Bigg[2\left\{(1-\phi)+\phi\left(\frac{\rho_s}{\rho_f}\right)\right\}\left(\begin{aligned}&-\left(\frac{1}{3}\right)(1-\phi)^{2.5}\left\{(1-\phi)+\phi\left[(\rho\beta)_s/(\rho\beta)_f\right]\right\}ab\\&+\left(\frac{1}{4}\right)(1-\phi)^{5}\left\{(1-\phi)+\phi\left[(\rho\beta)_s/(\rho\beta)_f\right]\right\}^2\end{aligned}\right)\\
&-3\left\{(1-\phi)+\phi\left(\frac{\rho_s}{\rho_f}\right)\right\}-\left(\frac{7}{24}\right)(1-\phi)^{2.5}\left\{(1-\phi)+\phi\left[(\rho\beta)_s/(\rho\beta)_f\right]\right\}ab\\
&+\left(\frac{(1-\phi)^5}{6}\right)\left\{(1-\phi)+\phi\left[(\rho\beta)_s/(\rho\beta)_f\right]\right\}^2\\
&+\left(\frac{\left\{(1-\phi)+\phi\left[(\rho\beta)_s/(\rho\beta)_f\right]\right\}Pr}{8}\right)\left\{\frac{1}{\left[(1-\phi)+\phi\left[(\rho c_p)_s/(\rho c_p)_f\right]\right]}\cdot\left[\frac{k_s+(m-1)k_f-(m-1)\phi(k_f-k_s)}{k_s+(m-1)k_f+\phi(k_f-k_s)}\right]\right\}ab\Bigg]\\
&-\left(\frac{(1-\phi)^5}{90}\right)\left\{(1-\phi)+\phi\left[(\rho\beta)_s/(\rho\beta)_f\right]\right\}a^2b\Bigg)\\
&+\left(\frac{\left\{(1-\phi)+\phi\left[(\rho\beta)_s/(\rho\beta)_f\right]\right\}Pr}{14}\right)\left\{\frac{1}{\left[(1-\phi)+\phi\left[(\rho c_p)_s/(\rho c_p)_f\right]\right]}\cdot\left[\frac{k_s+(m-1)k_f-(m-1)\phi(k_f-k_s)}{k_s+(m-1)k_f+\phi(k_f-k_s)}\right]\right\}\\
&\quad\left(\begin{aligned}&-\left(\frac{a^2Pr}{4}\right)\left\{\frac{1}{\left[(1-\phi)+\phi\left[(\rho c_p)_s/(\rho c_p)_f\right]\right]}\cdot\left[\frac{k_s+(m-1)k_f-(m-1)\phi(k_f-k_s)}{k_s+(m-1)k_f+\phi(k_f-k_s)}\right]\right\}b\\&+\left(\frac{(1-\phi)^{2.5}}{120}\right)\left\{(1-\phi)+\phi\left(\frac{\rho_s}{\rho_f}\right)\right\}a^2b\end{aligned}\right)\Bigg\}
\end{aligned}
$$

In the same manner, the expressions for *F [11], F[12], F[13], F[14], F[15]* are found, which are too large to be included in this paper. Also, using *p=0, 1, 2, 3…* in the above recursive relations in Eq. (21), we arrived at

$$\Theta[2]=0,\quad \Theta[3]=0$$

$$\Theta[4]=-\frac{Pr}{8}\left\{\frac{1}{\left[(1-\phi)+\phi\left[(\rho c_p)_s/(\rho c_p)_f\right]\right]}\left[\frac{k_s+(m-1)k_f-(m-1)\phi(k_f-k_s)}{k_s+(m-1)k_f+\phi(k_f-k_s)}\right]\right\}ab$$

$$\Theta[5]=\frac{Pr}{40}\left\{\begin{aligned}&\left\{\frac{1}{\left[(1-\phi)+\phi\left[(\rho c_p)_s/(\rho c_p)_f\right]\right]}\left[\frac{k_s+(m-1)k_f-(m-1)\phi(k_f-k_s)}{k_s+(m-1)k_f+\phi(k_f-k_s)}\right]\right\}\\&\cdot(1-\phi)^{2.5}\left[(1-\phi)+\phi\left[(\rho\beta)_s/(\rho\beta)_f\right]\right]b\end{aligned}\right\}$$

$$\Theta[6]=\frac{Pr}{120}\left\{\begin{array}{l}\left\{\dfrac{1}{\left[(1-\phi)+\phi\left[(\rho c_p)_s/(\rho c_p)_f\right]\right]}\left[\dfrac{k_s+(m-1)k_f-(m-1)\phi(k_f-k_s)}{k_s+(m-1)k_f+\phi(k_f-k_s)}\right]\right\}\\ \cdot(1-\phi)^{2.5}\left[(1-\phi)+\phi\left[(\rho\beta)_s/(\rho\beta)_f\right]\right]b^2\end{array}\right\}$$

$$\Theta[7]=-\frac{Pr}{14}\left\{\begin{array}{l}\left\{\dfrac{1}{\left[(1-\phi)+\phi\left[(\rho c_p)_s/(\rho c_p)_f\right]\right]}\left[\dfrac{k_s+(m-1)k_f-(m-1)\phi(k_f-k_s)}{k_s+(m-1)k_f+\phi(k_f-k_s)}\right]\right\}\\ \cdot\left(\begin{array}{l}-\dfrac{Pr}{4}\left\{\dfrac{1}{\left[(1-\phi)+\phi\left[(\rho c_p)_s/(\rho c_p)_f\right]\right]}\left[\dfrac{k_s+(m-1)k_f-(m-1)\phi(k_f-k_s)}{k_s+(m-1)k_f+\phi(k_f-k_s)}\right]\right\}a^2b\\ +\left(\dfrac{1}{120}\right)(1-\phi)^{2.5}\left[(1-\phi)+\phi\left[(\rho)_s/(\rho)_f\right]\right]a^2b\end{array}\right)\end{array}\right\}$$

$$\Theta[8]=-\frac{Pr^2}{128}\left\{\begin{array}{l}\left\{\dfrac{1}{\left[(1-\phi)+\phi\left[(\rho c_p)_s/(\rho c_p)_f\right]\right]}\left[\dfrac{k_s+(m-1)k_f-(m-1)\phi(k_f-k_s)}{k_s+(m-1)k_f+\phi(k_f-k_s)}\right]\right\}^2\\ \cdot(1-\phi)^{2.5}\left[(1-\phi)+\phi\left[(\rho\beta)_s/(\rho\beta)_f\right]\right]ab\end{array}\right\}$$

$$\Theta[9]=\frac{-Pr}{24}\left\{\begin{array}{l}\left\{\dfrac{1}{\left[(1-\phi)+\phi\left[(\rho c_p)_s/(\rho c_p)_f\right]\right]}\left[\dfrac{k_s+(m-1)k_f-(m-1)\phi(k_f-k_s)}{k_s+(m-1)k_f+\phi(k_f-k_s)}\right]\right\}\\ \cdot\left(\begin{array}{l}\left\{\begin{array}{l}\dfrac{Pr}{30}\left\{\dfrac{1}{\left[(1-\phi)+\phi\left[(\rho c_p)_s/(\rho c_p)_f\right]\right]}\dfrac{k_s+(m-1)k_f-(m-1)\phi(k_f-k_s)}{k_s+(m-1)k_f+\phi(k_f-k_s)}\right\}\\ \cdot(1-\phi)^{2.5}\left[(1-\phi)+\phi\left[(\rho\beta)_s/(\rho\beta)_f\right]\right]ab^2\end{array}\right\}\\ -\dfrac{Pr}{48}\left\{\begin{array}{l}\left\{\dfrac{1}{\left[(1-\phi)+\phi\left[(\rho c_p)_s/(\rho c_p)_f\right]\right]}\dfrac{k_s+(m-1)k_f-(m-1)\phi(k_f-k_s)}{k_s+(m-1)k_f+\phi(k_f-k_s)}\right\}\\ \cdot(1-\phi)^5\left[(1-\phi)+\phi\left[(\rho\beta)_s/(\rho\beta)_f\right]\right]^2b\end{array}\right\}\\ +\dfrac{(1-\phi)^{2.5}}{210}\left(\left(\begin{array}{l}2\left[(1-\phi)+\phi\left[(\rho)_s/(\rho)_f\right]\right]\left(\begin{array}{l}-\left(\dfrac{1}{3}\right)(1-\phi)^{2.5}a\left[(1-\phi)+\phi\left[(\rho\beta)_s/(\rho\beta)_f\right]\right]b\\ +\left(\dfrac{1}{4}\right)(1-\phi)^5\left[(1-\phi)+\phi\left[(\rho\beta)_s/(\rho\beta)_f\right]\right]^2\end{array}\right)\\ -3\left[(1-\phi)+\phi\left[(\rho)_s/(\rho)_f\right]\right]\left(\begin{array}{l}-\left(\dfrac{7}{24}\right)(1-\phi)^{2.5}\left[(1-\phi)+\phi\left[(\rho\beta)_s/(\rho\beta)_f\right]\right]ab\\ +\left(\dfrac{1}{6}\right)(1-\phi)^5\left[(1-\phi)+\phi\left[(\rho\beta)_s/(\rho\beta)_f\right]\right]^2\end{array}\right)\\ +\dfrac{Pr}{8}\left\{\begin{array}{l}\left\{\left[\dfrac{1}{\left[(1-\phi)+\phi\left[(\rho c_p)_s/(\rho c_p)_f\right]\right]}\right]\cdot\left[\dfrac{k_s+(m-1)k_f-(m-1)\phi(k_f-k_s)}{k_s+(m-1)k_f+\phi(k_f-k_s)}\right]\right\}\\ \cdot\left[(1-\phi)+\phi\left[(\rho\beta)_s/(\rho\beta)_f\right]\right]ab\end{array}\right\}\end{array}\right)b\right)\end{array}\right)\end{array}\right\}$$

$$
\begin{aligned}
\Theta[10] = -\frac{Pr}{4}&\left\{\frac{1}{\left[(1-\phi)+\phi\left[(\rho c_p)_s/(\rho c_p)_f\right]\right]}\cdot\left[\frac{k_s+(m-1)k_f-(m-1)\phi(k_f-k_s)}{k_s+(m-1)k_f+\phi(k_f-k_s)}\right]\right\}\\
&\left(\begin{aligned}
&-\frac{aPr}{4}\left\{\begin{aligned}&\left\{\frac{1}{\left[(1-\phi)+\phi\left[(\rho c_p)_s/(\rho c_p)_f\right]\right]}\cdot\left[\frac{k_s+(m-1)k_f-(m-1)\phi(k_f-k_s)}{k_s+(m-1)k_f+\phi(k_f-k_s)}\right]\right\}\\
&\cdot\left(\begin{aligned}&-\frac{Pr}{4}\left\{\frac{1}{\left[(1-\phi)+\phi\left[(\rho c_p)_s/(\rho c_p)_f\right]\right]}\cdot\left[\frac{k_s+(m-1)k_f-(m-1)\phi(k_f-k_s)}{k_s+(m-1)k_f+\phi(k_f-k_s)}\right]\right\}a^2b\\
&+\left(\frac{1}{120}\right)(1-\phi)^{2.5}\left[(1-\phi)+\phi\left[(\rho)_s/(\rho)_f\right]\right]a^2b\end{aligned}\right)\end{aligned}\right\}\\
&-\frac{3(1-\phi)^5Pr}{320}\left\{\frac{1}{\left[(1-\phi)+\phi\left[(\rho c_p)_s/(\rho c_p)_f\right]\right]}\cdot\left[\frac{k_s+(m-1)k_f-(m-1)\phi(k_f-k_s)}{k_s+(m-1)k_f+\phi(k_f-k_s)}\right]\right\}\left[(1-\phi)+\phi\left[(\rho\beta)_s/(\rho\beta)_f\right]\right]^2b^2\\
&-\frac{(1-\phi)^{2.5}a^3Pr}{120}\left[(1-\phi)+\phi\left[(\rho\beta)_s/(\rho\beta)_f\right]\right]\left\{\frac{1}{\left[(1-\phi)+\phi\left[(\rho c_p)_s/(\rho c_p)_f\right]\right]}\cdot\left[\frac{k_s+(m-1)k_f-(m-1)\phi(k_f-k_s)}{k_s+(m-1)k_f+\phi(k_f-k_s)}\right]\right\}b\\
&+\frac{(1-\phi)^{2.5}}{336}\left(\begin{aligned}&2\left\{\begin{aligned}&\left[(1-\phi)+\phi\left[(\rho\beta)_s/(\rho\beta)_f\right]\right]\cdot\\&\left(\begin{aligned}&\left(\frac{1}{12}\right)a^3(1-\phi)^{2.5}\left[(1-\phi)+\phi\left[(\rho\beta)_s/(\rho\beta)_f\right]\right]\\&+\left(\frac{1}{6}\right)(1-\phi)^5\left[(1-\phi)+\phi\left[(\rho\beta)_s/(\rho\beta)_f\right]\right]^2b\end{aligned}\right)\end{aligned}\right\}\\
&-3\left\{\begin{aligned}&\left[(1-\phi)+\phi\left[(\rho\beta)_s/(\rho\beta)_f\right]\right]\\&\cdot\left(\begin{aligned}&\left(\frac{11}{120}\right)a^3(1-\phi)^{2.5}\left[(1-\phi)+\phi\left[(\rho\beta)_s/(\rho\beta)_f\right]\right]\\&+\left(\frac{1}{8}\right)(1-\phi)^5\left[(1-\phi)+\phi\left[(\rho\beta)_s/(\rho\beta)_f\right]\right]^2b\end{aligned}\right)\end{aligned}\right\}\\
&-\frac{Pr}{40}\left\{\begin{aligned}&\left\{\frac{1}{\left[(1-\phi)+\phi\left[(\rho c_p)_s/(\rho c_p)_f\right]\right]}\cdot\left[\frac{k_s+(m-1)k_f-(m-1)\phi(k_f-k_s)}{k_s+(m-1)k_f+\phi(k_f-k_s)}\right]\right\}\\&\cdot\left[(1-\phi)+\phi\left[(\rho\beta)_s/(\rho\beta)_f\right]\right]^2(1-\phi)^{2.5}\end{aligned}\right\}b\end{aligned}\right)b
\end{aligned}\right)
\end{aligned}
$$

In addition, the expressions for $\Theta[11]$, $\Theta[12]$, $\Theta[13]$, $\Theta[14]$, $\Theta[15]$ are found in the same way but they are too large to be included in this paper. Using the definition in Eq. (17), the solutions of Eqs. (10) and (11) are given as

$$
\begin{aligned}
f(\eta) = F[0]+\eta F[1]+\eta^2F[2]+\eta^3F[3]+ +\eta^4F[4]+\eta^5F[5]\\
+\eta^6F[6]+\eta^7F[7]+\eta^8F[8]+\eta^9F[9]+\eta^{10}F[10]+\ldots
\end{aligned}
\tag{24}
$$

$$
\begin{aligned}
\theta(\eta) = \Theta[0]+\eta\Theta[1]+\eta^2\Theta[2]+\eta^3\Theta[3]+ +\eta^4\Theta[4]+\eta^5\Theta[5]\\
+\eta^6\Theta[6]+\eta^7\Theta[7]+\eta^8\Theta[8]+\eta^9\Theta[9]+\eta^{10}\Theta[10]+\ldots
\end{aligned}
\tag{25}
$$

The solutions of Eqs. (12) and (13) for a viscous fluid which does not have nanoparticles can be developed from Eqs. (24) and (25) if nanoparticle volume fraction is set to zero i.e. $\phi=0$.

4. The basic concept and the procedure of Padé Approximant

The limitations of power series methods to a small domain have been overcome by after-treatment techniques. These techniques increase the radius of convergence and accelerate the rate of convergence of a given series. Among the so-called after-treatment techniques, the Padé approximant technique has been widely applied in developing accurate analytical solutions to nonlinear problems of large or unbounded domain problems of infinite boundary conditions [30]. The Padé-approximant technique manipulates a polynomial approximation into a rational function of polynomials. Such a manipulation gives more information about the mathematical behavior of the solution. The basic procedures are as follows. Suppose that a function $f(\eta)$ is represented by a power series.

$$f(\eta)=\sum_{i=0}^{\infty} c_i \eta^i \tag{26}$$

This expression is the fundamental point of any analysis using Padé approximant. The notation $c_i, i=0,1,2,\ldots$ is reserved for the given set of coefficient and $f(\eta)$ is the associated function. [*L/M*] Padé approximant is a rational function defined as

$$f(\eta)=\frac{\sum_{i=0}^{L} a_i \eta^i}{\sum_{i=0}^{M} b_i \eta^i}=\frac{a_0+a_1\eta+a_2\eta^2+\ldots+a_L\eta^L}{b_0+b_1\eta+b_2\eta^2+\ldots+b_M\eta^M} \tag{27}$$

which has a Maclaurin expansion and agrees with equation (1) as far as possible. It is noticed that in Eq. (27), there are *L+1* numerator and *M+1* denominator coefficients. Therefore, there are *L+1* independent number of numerator coefficients, making *L+M+1* unknown coefficients in all. This number suggests that normally (*L/M*) is out of fit the power series Eq. (26) through the orders $1,\eta,\eta^2,\ldots,\eta^{L+M}$. In the notation of formal power series

$$\sum_{i=0}^{\infty} c_i \eta^i=\frac{a_0+a_1\eta+a_2\eta^2+\ldots+a_L\eta^L}{b_0+b_1\eta+b_2\eta^2+\ldots+b_M\eta^M}+\mathrm{O}(\eta^{L+M+1)} \tag{28}$$

which gives

$$(b_0+b_1\eta+b_2\eta^2+\ldots+b_M\eta^M)(c_0+c_1\eta+c_2\eta^2+\ldots)=a_0+a_1\eta+a_2\eta^2+\ldots+a_L\eta^L+\mathrm{O}(\eta^{L+M+1)} \tag{29}$$

Expanding the LHS and equating the coefficients of $\eta^{L+1},\eta^{L+2},\ldots,\eta^{L+M}$, we get

$$\begin{gathered}
b_M c_{L-M+1}+b_{M-1}c_{L-M+2}+b_{M-2}c_{L-M+3}+\ldots+b_2c_{L-1}+b_1c_L+b_0c_{L+1}=0\\
b_M c_{L-M+2}+b_{M-1}c_{L-M+3}+b_{M-2}c_{L-M+4}+\ldots+b_2c_L+b_1c_{L+1}+b_0c_{L+2}=0\\
b_M c_{L-M+3}+b_{M-1}c_{L-M+4}+b_{M-2}c_{L-M+5}+\ldots+b_2c_{L+1}+b_1c_{L+2}+b_0c_{L+3}=0\\
\ldots\\
b_M c_L+b_{M-1}c_{L+1}+b_{M-2}c_{L+2}+\ldots+b_2c_{L+M-2}+b_1c_{L+M-1}+b_0c_{L+M}=0
\end{gathered} \tag{30}$$

If $i<0, \mathrm{c}_i=0$ for consistency. Since $b_0=1$, Eq. (30) becomes a set of *M* linear equations for *M* unknown denominator coefficients.

$$\begin{pmatrix}
c_{L-M+1} & c_{L-M+2} & c_{L-M+3} & \cdots & c_L\\
c_{L-M+2} & c_{L-M+3} & c_{L-M+4} & \cdots & c_{L+1}\\
c_{L-M+3} & c_{L-M+4} & c_{L-M+4} & \cdots & c_{L+2}\\
\vdots & \vdots & \vdots & \vdots & \vdots\\
c_L & c_{L+1} & c_{L+2} & \cdots & c_{L+M-1}
\end{pmatrix}
\begin{pmatrix} b_M\\ b_{M-1}\\ b_{M-2}\\ \vdots\\ b_1\end{pmatrix}
=-\begin{pmatrix} c_{L+1}\\ c_{L+2}\\ c_{L+3}\\ \vdots\\ c_{L+M}\end{pmatrix} \tag{31}$$

From Eq. (31), b_i can be found. The numerator coefficients $a_0,a_1,a_2,\ldots,a_L$ follow immediately from Eq. (29) by equating the coefficient of $1,\eta,\eta^2,\ldots,\eta^{L+M}$ such that

$$\begin{aligned}
&a_0=c_0\\
&a_1=c_1+b_1c_0\\
&a_2=c_2+b_1c_1+b_2c_0\\
&a_3=c_3+b_1c_2+b_2c_1+b_3c_0\\
&a_4=c_4+b_1c_3+b_2c_2+b_3c_1+b_4c_0\\
&a_5=c_5+b_1c_4+b_2c_3+b_3c_2+b_4c_1+b_5c_0\\
&a_6=c_6+b_1c_5+b_2c_4+b_3c_3+b_4c_2+b_5c_1+b_6c_0\\
&\ldots\\
&a_L=c_L+\sum_{i=1}^{min[L/M]} b_i c_{L-i}
\end{aligned} \tag{32}$$

Eqs. (31) and (32) normally determine the Pade-numerator and denominator which are called Padé equations. The [L/M] Pade-approximant is constructed, which agrees with the equation in the power series through the order η^{L+M}. To obtain a diagonal Padé approximant of order [L/M], the symbolic calculus software Maple was used.

As mentioned previously, it should be noted that Δ and Ω in the solutions are unknown constants. In order to compute their values for extended large domains solutions, the power series as presented in Eqs. (24) and (25) were converted to rational functions using [18/18] Pade-approximation through the software Maple and then the infinite boundary conditions i.e. $\eta \to \infty, \quad f' = 0, \quad \theta = 0$ were applied. The resulting simultaneous equations were solved to obtain the values of Δ and Ω for the respective values of the physical and thermal properties of the nanofluids under considerations.

5. Flow and heat transfer parameters

In addition to determining the velocity and temperature distributions, it is often desirable to compute other physically important quantities (such as shear stress, drag, heat transfer rate, and heat transfer coefficient) associated with the free-convection flow and heat transfer problem. Consequently, two parameters, a flow parameter and a heat transfer parameter, were computed. The local heat transfer coefficient at the surface of the vertical plate can be obtained from

5.1 Fluid flow parameter

Skin friction coefficient

$$c_f = \frac{\tau_w}{\rho_{nf} u^2} = \frac{\mu_{nf} \left. \frac{\partial u}{\partial y} \right|_{y=0}}{\rho_{nf} u^2} = \frac{\mu_{nf} \left. \left(\frac{\partial u}{\partial \eta} \cdot \frac{\partial \eta}{\partial y} \right) \right|_{y=0}}{\rho_{nf} u^2} \tag{33}$$

After the dimensionless exercise,

$$c_f \left(Re_x \right)^{1/2} = \frac{f''(0)}{(1-\phi)^{2.5}}$$

$$c_f \left(Re_x \right)^{1/2} \frac{\tau_w}{\left(4Gr_x^3 \right)^{1/4} (\nu\mu)} = f''(0) \frac{f''(0)}{(1-\phi)^{2.5}}$$

5.2 Heat transfer parameter

Heat transfer coefficient

$$h_x = -\frac{k_{nf}}{T_w - T_\infty} \left(\frac{\partial T}{\partial y} \right)_{y=0} = -k_{nf} \theta'(0) \frac{1}{x} \left(\frac{1}{4} Gr_x \right)^{1/4} \tag{34}$$

The local Nusselt number is

$$\begin{aligned} Nu_x &= \frac{h_x x}{k_{nf}} = -\left(\frac{x}{T_w - T_\infty} \right) \left(\frac{\partial T}{\partial y} \right)_{y=0} = -\theta'(0) \left(\frac{1}{4} Gr_x \right)^{1/4} \\ Nu_x &= -\frac{\theta'(0)}{\sqrt{2}} Gr_x^{1/4} = f\left((Pr) Gr_x^{1/4} \right) \end{aligned} \tag{35}$$

where $\phi(Pr) = -\theta'(0)/\sqrt{2}$ is a function of Prandtl number. The dependence of ϕ on the Prandtl number is evidenced by Eq. (35). It could also be shown that

$$\frac{Nu_x}{\left(Re_x \right)^{1/2}} = -\frac{k_{nf}}{k_f} \theta'(0) = -\left[\frac{k_s + (m-1)k_f - (m-1)\phi(k_f - k_s)}{k_s + (m-1)k_f + \phi(k_f - k_s)} \right] \theta'(0) \tag{36}$$

where Re_x and Gr_x are the local Reynolds and Grashof numbers defined as:

$$Re_x = \frac{ux}{\nu_{nf}} \quad \text{and} \quad Gr_x = \frac{g\beta(T_w - T_\infty)x^3}{\nu^3}$$

6. Results and discussion

In this section, the solutions of DTM with [18/18] Padé approximation are presented graphically and the comparison of the present results with the previous results in literature are presented in tabular forms. Tables 1-16 present various comparisons of results of the present study and the previous works for viscous fluid i.e. when the volume fraction of the nanoparticle is zero (*ϕ=0*). It could be seen from the tables that there are excellent agreements between the past results and those of the present study. Moreover, the tables present the effects of the Prandtl number on the flow and heat transfer processes.

Table 1. Comparison of results for the skin friction parameter, $f''(0)$

Pr	Sparrow & Gregg [5]	Kuiken[8]	Present study
0.003	1.0223	1.0151	1. 0224
0.008	0.9955	0.9801	0.9955
0.020	0.9590	0.9284	0.9591
0.030	0.9384	0.8966	0.9384

Table 2. Comparison of results of $f(\infty)$

Pr	Sparrow & Gregg [5]	Kuiken[8]	Present study
0.003	8.7060	8.8763	8.7061
0.008	5.4018	5.4152	5.4017
0.020	3.4093	3.4055	3.4092
0.030	2.7878	2.7710	2.7878

Table 3. Comparison of results of $Nu_x/(G_x Pr^2)^{\frac{1}{4}} = -\theta'(0)$

Pr	Sparrow & Gregg [5]	Kuiken[8]	Present study
0.003	0.5827	0.5827	0.5827
0.008	0.5729	0.5714	0.5728
0.020	0.5582	0.5546	0.5583
0.030	0.5497	0.5443	0.5497

Table 4. Comparison of results of $f(\eta)$, $f'(\eta)$ and $f''(\eta)$ at Pr=0.01

η	$f(\eta)$		$f'(\eta)$		$f''(\eta)$	
	Ostrach[2]	Present study	Ostrach[2]	Present study	Ostrach[2]	Present study
0.0	0.0000	0.0000	0.0000	0.0000	0.9862	0.9845
1.0	0.3376	0.3376	0.5379	0.5379	0.1734	0.1734
2.0	0.9023	0.9023	0.5535	0.5535	0.0641	0.0641
3.0	1.4200	1.4200	0.4810	0.4810	0.0719	0.0719
4.0	1.8665	1.8665	0.4136	0.4136	0.0629	0.0629
5.0	2.2501	2.2501	0.3548	0.3548	0.0549	0.0549
6.0	2.5787	2.5787	0.3035	0.3035	0.0479	0.0479
7.0	2.8593	2.8593	0.2586	0.2586	0.0419	0.0419
9.0	3.2999	3.2999	0.1853	0.1853	0.0319	0.0319
11	3.6123	3.6123	0.1297	0.1297	0.0241	0.0241
13	3.8276	3.8276	0.0877	0.0877	0.0181	0.0181
16	4.0204	4.0204	0.0441	0.0441	0.0114	0.0114
20	4.1226	4.1226	0.0108	0.0108	0.0057	0.0057
22	4.1343	4.1343	0.0015	0.0015	0.0037	0.0037

Table 5. Comparison of results of $f(\eta)$, $f'(\eta)$ and $f''(\eta)$ at Pr=1

η	$f(\eta)$		$f'(\eta)$		$f''(\eta)$	
	Ostrach[2]	Present study	Ostrach[2]	Present study	Ostrach[2]	Present study
0.0	0.0000	0.0000	0.0000	0.0000	0.6421	0.6421
1.0	0.1809	0.1809	0.2502	0.2502	-0.0263	-0.0263
2.0	0.3859	0.3859	0.1450	0.1450	-0.1233	-0.1233
3.0	0.4791	0.4791	0.0524	0.0524	-0.0602	-0.0602
4.0	0.5096	0.5096	0.0151	0.0151	- 0.0202	-0.0202
5.0	0.5177	0.5177	0.0035	0.0035	-0.0057	-0.0057
6.0	0.5194	0.5194	0.0004	0.0004	-0.0014	-0.0014

Table 6. Comparison of results of $f(\eta)$, $f'(\eta)$ and $f''(\eta)$ at Pr=2

η	$f(\eta)$		$f'(\eta)$		$f''(\eta)$	
	Ostrach[2]	Present study	Ostrach[2]	Present study	Ostrach[2]	Present study
0.0	0.0000	0.0000	0.0000	0.0000	0.5713	0.5712
1.0	0.1508	0.1508	0.1994	0.1994	-0.0440	-0.0440
2.0	0.3066	0.3066	0.1050	0.1050	-0.0960	-0.0960
3.0	0.3731	0.3731	0.0373	0.0373	-0.0416	-0.0416
4.0	0.3953	0.3953	0.0018	0.0018	-0.0138	-0.0138
5.0	0.4023	0.4023	0.0037	0.0037	-0.0042	-0.0042
7.0	0.4053	0.4053	0.0005	0.0005	-0.0004	-0.0004
8.0	0.4056	0.4056	0.0002	0.0002	-0.0001	-0.0001
9.0	0.4058	0.4058	0.0001	0.0001	0.0000	0.0000
10.0	0.4059	0.4059	0.0001	0.0001	0.0000	0.0000
11.0	0.4059	0.4059	0.0001	0.0001	0.0000	0.0000

Table 7. Comparison of results of $f(\eta)$, $f'(\eta)$ and $f''(\eta)$ at Pr=10

η	$f(\eta)$		$f'(\eta)$		$f''(\eta)$	
	Ostrach[2]	Present study	Ostrach[2]	Present study	Ostrach[2]	Present study
0.0	0.0000	0.0000	0.0000	0.0000	0.4192	0.4191
1.0	0.0908	0.0908	0.1066	0.1066	-0.0462	-0.0462
2.0	0.1714	0.1714	0.0567	0.0567	-0.0400	-0.0400
3.0	0.2119	0.2119	0.0276	0.0276	-0.0201	-0.0201
4.0	0.2314	0.2314	0.0132	0.0132	-0.0098	-0.0098
5.0	0.2408	0.2408	0.0063	0.0063	-0.0047	-0.0047
7.0	0.2474	0.2474	0.0014	0.0014	-0.0011	-0.0011
8.0	0.2484	0.2484	0.0007	0.0007	-0.0005	-0.0005
9.0	0.2489	0.2489	0.0003	0.0003	-0.0002	-0.0002
10.0	0.2491	0.2491	0.0002	0.0002	-0.0001	-0.0001

Table 8. Comparison of results of $f(\eta)$, $f'(\eta)$ and $f''(\eta)$ at Pr=100

η	$f(\eta)$		$f'(\eta)$		$f''(\eta)$	
	Ostrach[2]	Present study	Ostrach[2]	Present study	Ostrach[2]	Present study
0.0	0.0000	0.0000	0.0000	0.0000	0.2517	0.2517
1.0	0.0371	0.0371	0.0385	0.0385	-0.0140	-0.0140
2.0	0.0692	0.0692	0.0265	0.0265	-0.0101	-0.0101
3.0	0.0912	0.0912	0.0180	0.0180	-0.0071	-0.0071
4.0	0.1061	0.1061	0.0121	0.0121	-0.0049	-0.0049
6.0	0.1226	0.1226	0.0053	0.0053	-0.0022	-0.0022
8.0	0.1297	0.1297	0.0022	0.0022	-0.0010	-0.0010
9.0	0.1315	0.1315	0.0014	0.0014	-0.0007	-0.0007
10.0	0.1326	0.1326	0.0008	0.0008	-0.0005	-0.0005
11.0	0.1332	0.1332	0.0004	0.0004	-0.0003	-0.0003
12.0	0.1335	0.1335	0.0002	0.0002	-0.0002	-0.0002
13.0	0.1336	0.1335	0.0000	0.0000	-00001	-0.0001

Table 9. Comparison of results of $f(\eta)$, $f'(\eta)$ and $f''(\eta)$ at Pr=1000

η	$f(\eta)$		$f'(\eta)$		$f''(\eta)$	
	Ostrach[2]	Present study	Ostrach[2]	Present study	Ostrach[2]	Present study
0.0	0.0000	0.0000	0.0000	0.0000	0.1450	0.1450
1.0	0.0135	0.0135	0.0136	0.0136	-0.0027	-0.0027
3.0	0.0358	0.0358	0.0090	0.0090	-0.0019	-0.0019
5.0	0.0912	0.0912	0.0180	0.0180	-0.0071	-0.0071
7.0	0.0603	0.0603	0.0039	0.0039	-0.0008	-0.0008
8.0	0.0638	0.0638	0.0032	0.0032	-0.0007	-0.0007
10.0	0.0691	0.0691	0.0022	0.0022	-0.0004	-0.0004
12.0	0.0727	0.0727	0.0015	0.0015	-0.0003	-0.0003
14.0	0.0752	0.0752	0.0011	0.0011	-0.0002	-0.0002
16.0	0.0771	0.0771	0.0008	0.0008	-0.0001	-0.0001
18.0	0.0786	0.0786	0.0007	0.0007	0.0000	0.0000
20.0	0.0798	0.0798	0.0006	0.0006	00000	0.0000
22.0	0.0809	0.0809	0.0005	0.0005	0.0000	0.0000

Table 10. Comparison of results of $\theta(\eta)$, and $\theta'(\eta)$ at *Pr=0.01*

η	$\theta(\eta)$		$\theta'(\eta)$	
	Ostrach[2]	Present study	Ostrach[2]	Present study
0.0	1.0000	1.0000	-0.0812	-0.0812
1.0	0.9189	0.9189	-0.0809	-0.0809
2.0	0.8387	0.8387	-0.0794	-0.0794
3.0	0.7606	0.7606	-0.0766	-0.0766
4.0	0.6857	0.6857	-0.0720	-0.0720
5.0	0.6149	0.6149	-0.0686	-0.0686
6.0	0.5487	0.5487	-0.0638	-0.0638
7.0	0.4874	0.4874	-0.0588	-0.0588
9.0	0.3799	0.3799	-0.0489	-0.0489
11.0	0.2915	0.2915	-0.0397	-0.0397
13.0	0.2202	0.2202	-0.0317	-0.0317
16.0	0.1399	0.1399	-0.0223	-0.0223
20.0	0.0894	0.0894	-0.0137	-0.0137
21.0	0.0565	0.0565	-0.0121	-0.0121
22.0	0.0452	0.0452	-0.0107	-0.0107

Table 11. Comparison of results of $\theta(\eta)$, and $\theta'(\eta)$ at *Pr=1*

η	$\theta(\eta)$		$\theta'(\eta)$	
	Ostrach[2]	Present study	Ostrach[2]	Present study
0.0	1.0000	1.0000	-0.5671	-0.5671
1.0	0.4638	0.4638	-0.4589	-0.4589
2.0	0.1422	0.1422	-0.1907	-0.1907
3.0	0.0339	0.0339	-0.0509	-0.0509
4.0	0.0072	0.0072	-0.0115	-0.0115
5.0	0.0014	0.0014	-0.0024	-0.0024
6.0	0.0002	0.0002	-0.0005	-0.0005

Table 12. Comparison of results of $\theta(\eta)$, and $\theta'(\eta)$ at *Pr=2*

η	$\theta(\eta)$		$\theta'(\eta)$	
	Ostrach[2]	Present study	Ostrach[2]	Present study
0.0	1.0000	1.0000	-0.7165	-0.7165
1.0	0.3476	0.3476	-0.5002	-0.5002
2.0	0.0592	0.0592	-0.1207	-0.1207
3.0	0.0066	0.0066	-0.0152	-0.0152
4.0	0.0007	0.0007	-0.0015	-0.0015
5.0	0.0001	0.0001	-0.0686	-0.0686
6.0	0.5487	0.5487	-0.0001	-0.0001
7.0	0.0000	0.0000	0.0000	0.0000
8.0	0.0000	0.0000	0.0000	0.0000
9.0	0.0000	0.0000	0.0000	0.0000
10.0	0.0000	0.0000	0.0000	0.0000

Table 13. Comparison of results of $\theta(\eta)$, and $\theta'(\eta)$ at *Pr=10*

η	$\theta(\eta)$		$\theta'(\eta)$	
	Ostrach[2]	Present study	Ostrach[2]	Present study
0.0	1.0000	1.0000	-1.1694	-1.1694
1.0	0.1090	0.1090	-0.3753	-0.3753
2.0	0.0012	0.0012	-0.0065	-0.0065
3.0	0.0000	0.0000	0.0000	0.0000
4.0	0.0000	0.0000	0.0000	0.0000
5.0	0.0000	0.0000	0.0000	0.0000
7.0	0.0000	0.0000	0.0000	0.0000
8.0	0.0000	0.0000	0.0000	0.0000
9.0	0.0000	0.0000	0.0000	0.0000
10.0	0.0000	0.0000	0.0000	0.0000

Table 14. Comparison of results of $\theta(\eta)$, and $\theta'(\eta)$ at *Pr=100*

η	$\theta(\eta)$		$\theta'(\eta)$	
	Ostrach[2]	Present study	Ostrach[2]	Present study
0.0	1.0000	1.0000	-2.1910	-2.1910
1.0	0.0012	0.0012	-0.0149	-0.0149
2.0	0.0000	0.0000	0.0000	0.0000
3.0	0.0000	0.0000	0.0000	0.0000
4.0	0.0000	0.0000	0.0000	0.0000
7.0	0.0000	0.0000	0.0000	0.0000
8.0	0.0000	0.0000	0.0000	0.0000
9.0	0.0000	0.0000	0.0000	0.0000
10.0	0.0000	0.0000	0.0000	0.0000
11.0	0.0000	0.0000	0.0000	0.0000
12.0	0.0000	0.0000	0.0000	0.0000
13.0	0.0000	0.0000	0.0000	0.0000

It could be stablished that the nonlinear partial differential equations are the same in all aspects as the present problems under investigation with that of Mosta et al. [17]. However, there are slight differences between the transformed nonlinear ordinary differential equations in Mosta et al. [17]'s work for Eq. (7) and the developed Eqs. (12) and (13) in this study (where the volume fraction of the nanoparticle is set to zero) due to the differences in the adopted similarity variables. It is shown that using the DTM-Padé approximant, as applied in this work to the transformed nonlinear ordinary differential equations in Mosta et al. [17], excellent agreements are recorded between the results of the present study and that of Mosta et al. [17] and Kuiken [52], as shown in Tables 17 and 18.

Table 15. Comparison of results of $\theta(\eta)$, and $\theta'(\eta)$ at *Pr=1000*

η	$\theta(\eta)$		$\theta'(\eta)$	
	Ostrach[2]	Present study	Ostrach[2]	Present study
0.0	1.0000	1.0000	-3.9660	-3.9660
1.0	0.0000	0.0000	0.0000	0.0000
3.0	0.0000	0.0000	0.0000	0.0000
5.0	0.0000	0.0000	0.0000	0.0000
7.0	0.0000	0.0000	0.0000	0.0000
8.0	0.0000	0.0000	0.0000	0.0000
10.0	0.0000	0.0000	0.0000	0.0000
20.0	0.0000	0.0000	0.0000	0.0000
22.0	0.0000	0.0000	0.0000	0.0000
23.0	0.0000	0.0000	0.0000	0.0000

Table 16. Comparison of results for Comparison of results of $f''(\eta)$ and $\theta'(\eta)$ at different Prandtl numbers

Pr	Kuo[43]		Na and Hibb[12]		Present study	
	$f''(0)$	$\theta'(0)$	$f''(0)$	$\theta'(0)$	$f''(0)$	$\theta'(0)$
0.72	0.6760	-0.5046	0.6760	-0.5046	0.6760	-0.5046
0.60	0.6947	-0.4721	0.6946	-0.4725	0.6947	-0.4721
0.50	0.7132	-0.4411	0.7131	-0.4420	0.7132	-0.4411
0.40	0.7356	-0.4053	0.7354	-0.4066	0.7356	-0.4053
0.30	0.7636	-0.3623	0.7633	-0.3641	0.7636	-0.3623
0.20	0.8015	-0.3078	0.8009	-0.3101	0.8015	-0.3078
0.10	0.8600	-0.2298	0.8590	-0.2326	0.8600	-0.2298
0.06	0.8974	-0.1834	0.8961	-0.1864	0.8974	-0.1834
0.04	0.9233	-0.1526	0.9221	-0.1556	0.9233	-0.1526
0.01	0.9845	-0.0832	0.9887	-0.0817	0.9885	-0.0832
1.00	0.6421	-0.5671	0.6421	-0.5671	0.6421	-0.5671
1.10	0.6323	-0.5862	0.6323	-0.5860	0.6323	-0.5862
1.20	0.6233	-0.6040	0.6234	-0.6036	0.6233	-0.6040
1.30	0.6151	-0.6208	0.6152	-0.6202	0.6151	-0.6208
1.40	0.6075	-0.6365	0.6076	-0.6358	0.6075	-0.6365
1.50	0.6005	-0.6515	0.6006	-0.6506	0.6005	-0.6515
1.60	0.5939	-0.6656	0.5940	-0.6646	0.5939	-0.6656
1.70	0.5877	-0.6792	0.5879	-0.6780	0.5877	-0.6792
1.80	0.5819	-0.6921	0.5821	-0.6908	0.5819	-0.6921
1.90	0.5764	-0.7045	0.5767	-0.7031	0.5764	-0.7045
2.00	0.5712	-0.7164	0.5715	-0.7149	0.5712	-0.7164
2.00	0.5712	-0.7164	0.5713	-0.7165	0.5712	-0.7164
3.00	0.5308	-0.8154	0.5312	-0.8145	0.5308	-0.8154
4.00	0.5029	-0.8914	0.5036	-0.8898	0.5029	-0.8914
5.00	0.4817	-0.9539	0.4827	-0.9517	0.4817	-0.9539
6.00	0.4648	-1.0073	0.4660	-1.0047	0.4648	-1.0073
7.00	0.4507	-1.0542	0.4522	-1.0512	0.4507	-1.0542
8.00	0.4387	-1.0961	0.4405	-1.0930	0.4387	-1.0961
9.00	0.4283	-1.1342	0.4304	-1.1309	0.4283	-1.1342
10.00	0.4191	-1.1692	0.4215	-1.1658	0.4191	-1.1692

Table 17. Comparison of results of $f''(\eta)$ at different Prandtl number

Pr	Kuiken [52]	Mosta [17]	Present study
0.001	1.12313813	1.12313813	1.12313813
0.01	1.06338086	1.06338086	1.06338086
0.1	0.92408304	0.92408304	0.92408304
1	0.69321163	0.69321163	0.69321163
10	0.44711652	0.44711652	0.44711652
100	0.26452354	0.26452354	0.26452354
1000	0.15129020	0.15129020	0.15129020
10000	0.08554085	0.08554085	0.08554085

Having established the high accuracy of the differential transformation method coupled with the Padé-approximant technique, parametric studies are carried out and the results are presented in the subsequent sections. The variations of nanoparticle volume fraction with dynamic viscosity and thermal conductivity ratios of Copper (II) Oxide-water nanofluid are shown in Figs. 2 and 3, respectively. Also, Fig. 3 shows the effects of nanoparticle shape on thermal conductivity ratio. It is depicted in the figure that the thermal conductivity of nanofluid varies linearly and is increased by increasing the nanoparticle volume fraction. It is also observed that the suspensions of particles with a high shape factor or low sphericity have higher thermal conductivity ratio of the nanofluid. Spherical shape nanoparticles have the lowest thermal conductivity ratio and lamina shape nanoparticles have the highest thermal conductivity ratio. The effects of the flow and heat transfer controlling parameters on the velocity and temperature distributions are shown in Figs. 4–17 for different shapes, types and volume-fractions of nanoparticles at Prandtl numbers 0.01-1000.

Table 18. Comparison of results of $-\theta'(0)$ at different Prandtl number

Pr	Kuiken [52]	Mosta et al. [17]	Mosta et al. [17]	Present study (DTM-Pade)
0.001	0.04680746	0.04680746	0.04680746	0.04680746
0.01	0.13576074	0.13576074	0.13576074	0.13576074
0.1	0.35005967	0.35005967	0.35005967	0.35005967
1	0.76986120	0.76986120	0.76986119	0.76986120
10	1.49709921	1.49709921	1.49709921	1.49709921
100	2.74688550	2.74688550	2.74688549	2.74688550
1000	4.93494763	4.93494763	4.93494756	4.93494763
10000	8.80444927	8.80444927	8.80444960	8.80444960

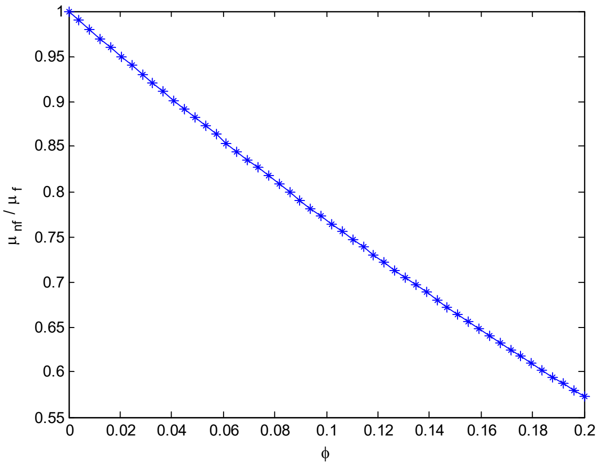

Fig. 2. Variation of nanofluid dynamic viscosity ratio with nanoparticle volume fraction

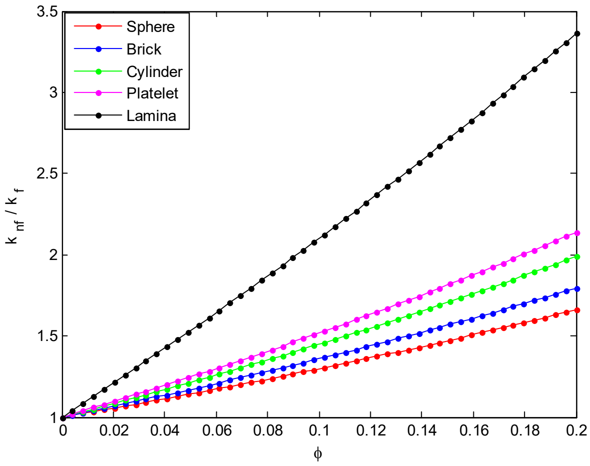

Fig. 3. Effects of nanoparticle shape on thermal conductivity ratio of nanofluid

(a) velocity profile (b) temperature profile

Fig. 5. Effects of Prandtl number when ϕ=0.020

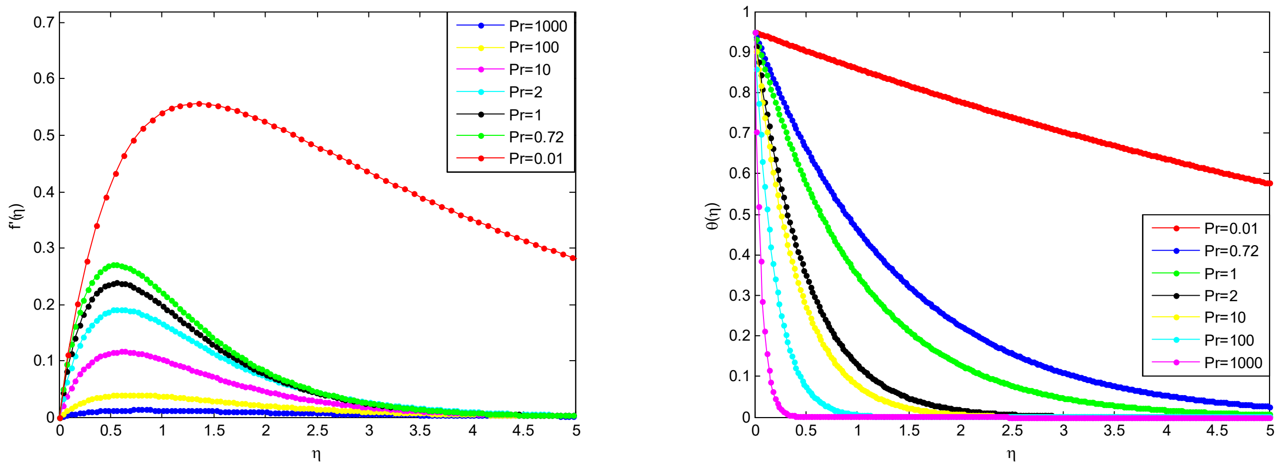

(a) velocity profile (b) temperature profile

Fig. 6. Effects of Prandtl number when ϕ=0.040

6.1 Effect of nanoparticle volume fraction on nanofluid velocity and temperature distributions for different values of Prandtl number

Figs. 5-8 show the effects of nanoparticle concentration/volume fraction and Prandtl number on velocity and temperature profiles of Copper (II) Oxide-water nanofluid. The figures indicate that as the volume-fraction or concentration of the nanoparticle in the nanofluid increases, the velocity decreases. However, an opposite trend or behavior is observed in the temperature profile, i.e. the nanofluid temperature increases as the volume-fraction of the nanoparticles in the basefluid increases. This is because the solid volume fraction has significant impacts on the thermal conductivity. The increased volume fraction of nanoparticles in basefluid results in higher thermal conductivity of the basefluid, which increases the heat enhancement capacity of the basefluid. Also, one of the possible reasons for the enhancement of heat transfer in nanofluids can be explained by the high concentration of nanoparticles in the thermal boundary layer at the wall side through the migration of nanoparticles. It should also be stated that the thickness of thermal boundary layer rises by increasing the values of nanoparticle volume fraction. Consequently, this can reduce the velocity of the nanofluid as the shear stress and skin friction are increased. The figures also show the effects of Prandtl number (Pr) on the velocity and temperature profiles. It is indicated that the velocity of the nanofluid decreases as the Pr increases but the temperature of the nanofluid increases as the Pr increases. This is because the nanofluid with higher Prandtl number has a relatively low thermal conductivity, which reduces conduction, and thereby reduces the thermal boundary-layer thickness, and as a consequence, increases the heat transfer rate at the surface. For the case of the fluid velocity that decreases by increasing Pr, the reason is that the fluid of the higher Prandtl number is a more viscous fluid, which increases the boundary-layer thickness and thus reduces the shear stress and, consequently, retards the flow of the nanofluid. Also, it can be seen that the velocity distribution for small values of Prandtl number consists of two distinct regions. A thin region near the wall of the plate where there are large velocity gradients due to viscous effects and a region where the velocity gradients are small compared with those near the wall. In the later region, the viscous effects are negligible and the flow of fluid in the region can be considered to be inviscid. Also, this region tends to create uniform accelerated flow at the surface of the plate.

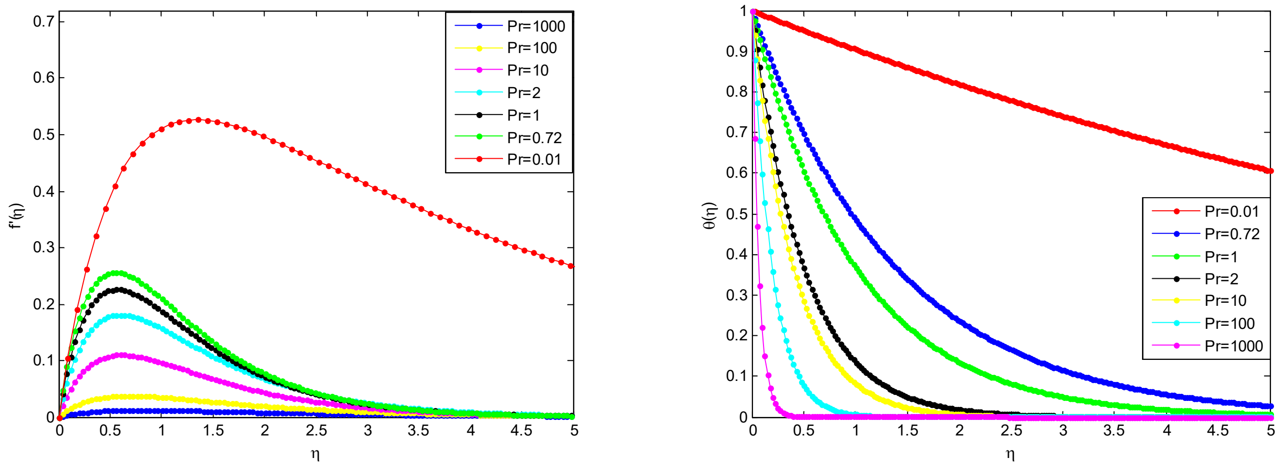

(a) velocity profile (b) temperature profile

Fig. 7. Effects of Prandtl number when ϕ=0.060

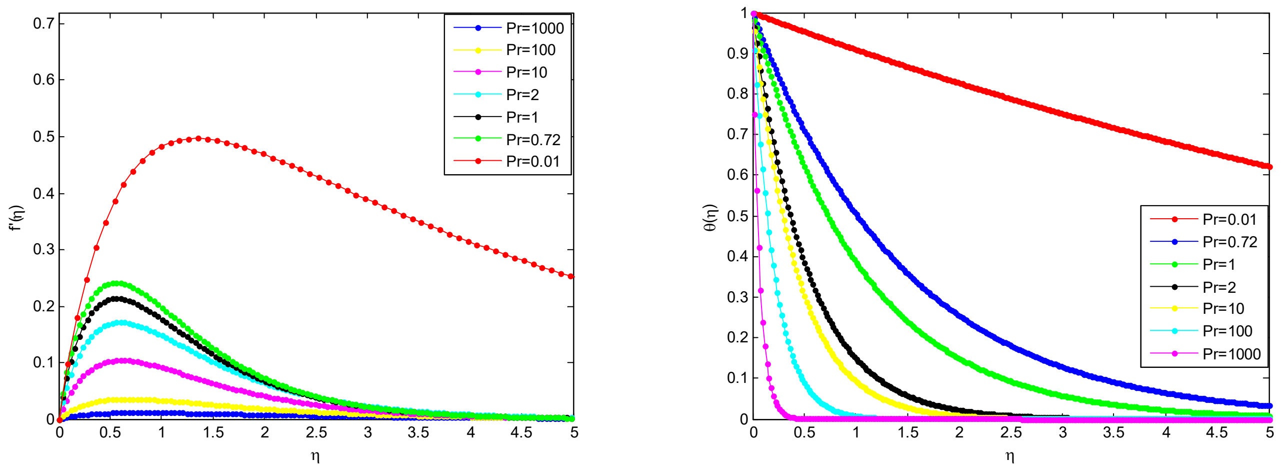

(a) velocity profile (b) temperature profile

Fig. 8. Effects of Prandtl number when ϕ=0.080

The use of nanoparticles in the fluids exhibited better properties relating to the heat transfer of fluid than heat transfer enhancement through the use of suspended millimeter- or micrometer-sized particles which potentially cause some severe problems, such as abrasion, clogging, high pressure drop, and sedimentation of particles. The very low concentration applications and nanometer-sized properties of nanoparticles in basefluid prevent the sedimentation in the flow that may clog the channel. It should be added that the theoretical prediction of enhanced thermal conductivity of the basefluid and the prevention of clogging, abrasion, high pressure drop and sedimentation through the addition of nanoparticles in basefluid have been supported with experimental evidence in the literature.

6.2 Effect of nanoparticle shape on nanofluid velocity and temperature distributions

It has been observed experimentally that the nanoparticle shape has significant impacts on the thermal conductivity. Therefore, the effects of nanoparticle shape at different values of Prandtl number on the velocity and temperature profiles of

Copper (II) Oxide-water nanofluid are shown in Figs. 9-13. It is indicated that the maximum decrease in velocity and the maximum increase in temperature are caused by lamina, platelets, cylinder, bricks, and sphere, respectively. It is observed that lamina-shaped nanoparticles have maximum velocity whereas spherical shaped nanoparticles have a better enhancement on heat transfer than other nanoparticle shapes. In fact, it is in accordance with the physical expectation since it is well known that the lamina nanoparticle has greater shape factor than other nanoparticles of different shapes. Therefore, the lamina nanoparticle comparatively gains maximum temperature than others. The decrease in velocity is maximum in spherical nanoparticles compared with other shapes. The enhancement observed at lower volume fractions for non-spherical particles is attributed to the percolation chain formation, which perturbs the boundary layer and thereby increases the local Nusselt number values.

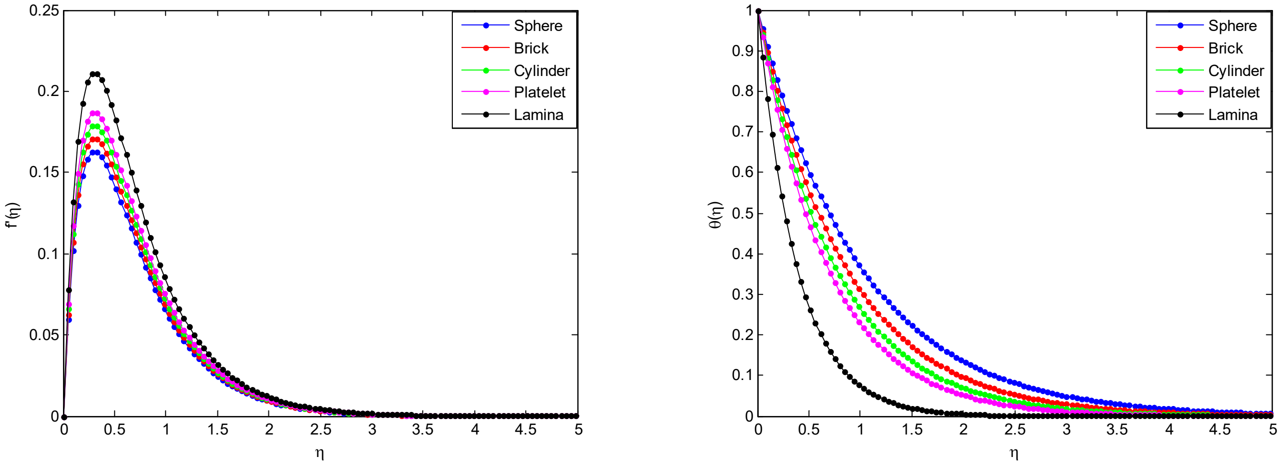

(a) velocity distribution (b) temperature distribution

Fig. 9. Effects of nanoparticle shapes on the nanofluid

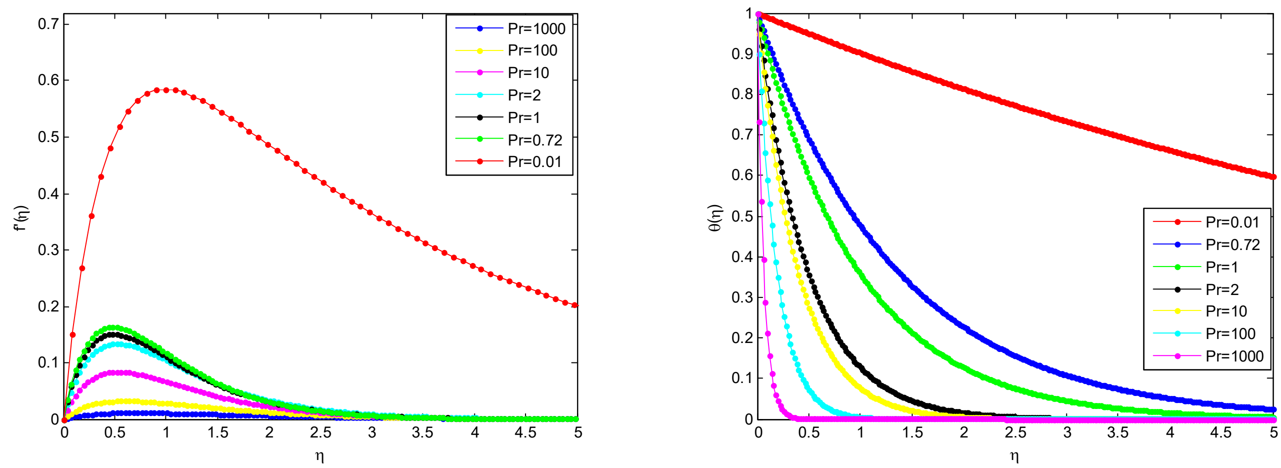

(a) velocity profile (b) temperature profile

Fig. 10. Effects of Prandtl number for spherical shape nanoparticle

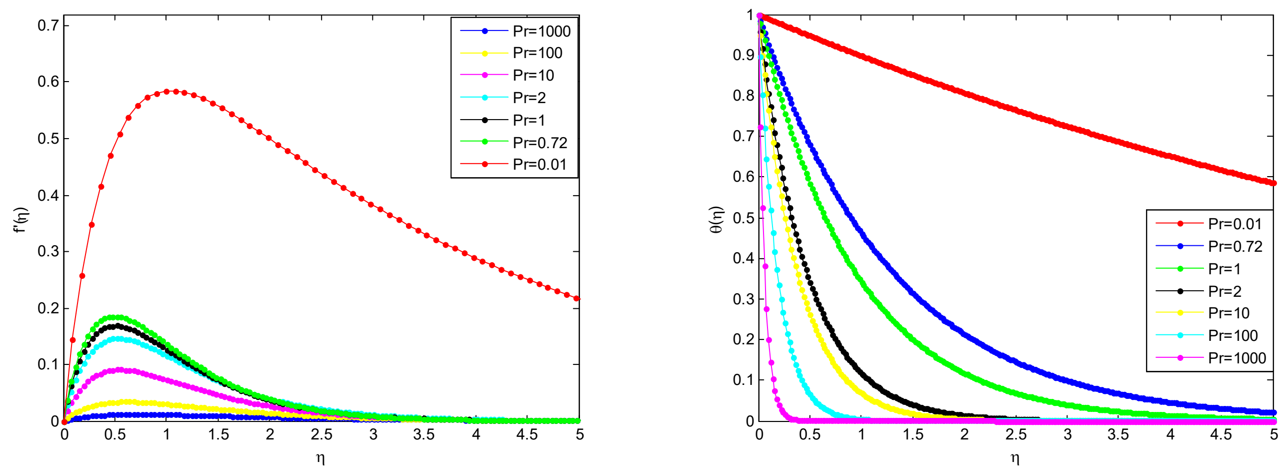

(a) velocity profile (b) temperature profile

Fig. 10. Effects of Prandtl number for brick shape nanoparticle

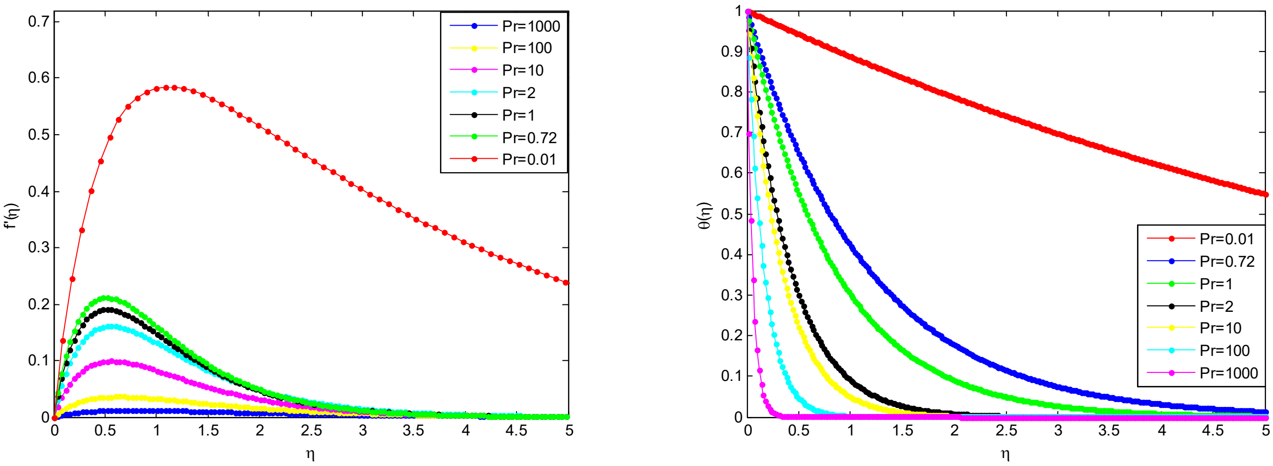

(a) velocity profile (b) temperature profile

Fig. 11. Effects of Prandtl number for cylindrical shape nanoparticle

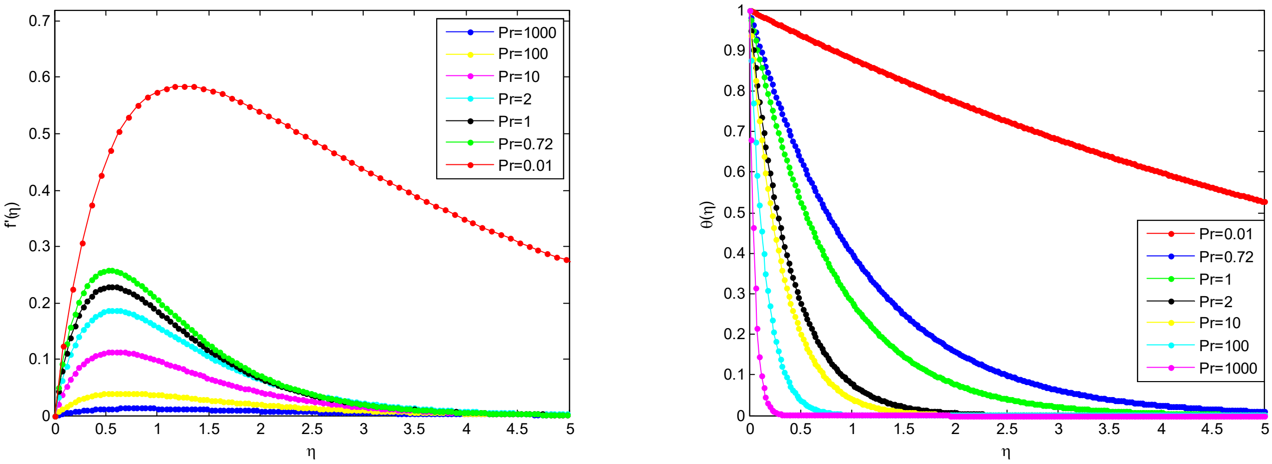

(a) velocity profile (b) temperature profile

Fig. 12. Effects of Prandtl number for platelet shape nanoparticle

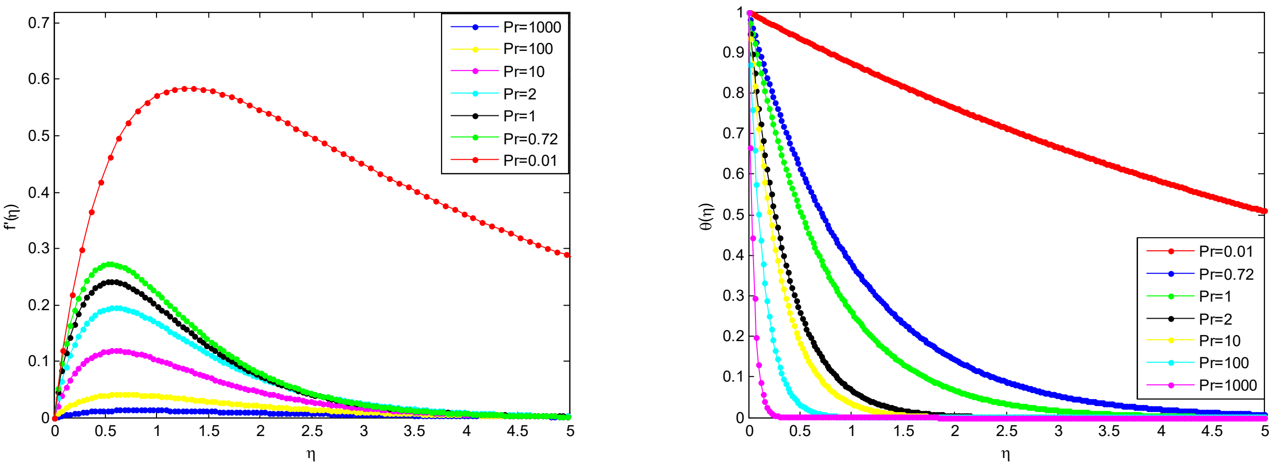

(a) velocity profile (b) temperature profile

Fig. 13. Effects of Prandtl number for lamina shape nanoparticle

It is evident from this study that proper choice of nanoparticles will be helpful in controlling velocity and heat transfer. It is also observed that irreversibility process can be reduced by using nanoparticles, especially the spherical particles. This can potentially result in higher enhancement in the thermal conductivity of a nanofluid containing elongated particles compared to the one containing spherical nanoparticle, as exhibited by the experimental data in the literature.

6.3 Effect of nanoparticle type on nanofluid velocity and temperature distribution

The variations of the velocity and temperature profiles against η for various types of nanoparticles (TiO2, CuO, Al2O3 and

SWCNTs) are shown in Figs. 14-17. Using a common basefluid for all the nanoparticle types, it is observed that the maximum decrease in velocity and maximum increase in temperature are caused by TiO2, CuO, Al2O3 and SWCNTs, respectively. It is observed that SWCNT nanoparticles carry maximum decrease in velocity but have a better enhancement on heat transfer than other nanoparticle shapes. In complete accordance with the physical expectations, the SWCNT nanoparticles have a higher thermal conductivity than other types of nanoparticles. As a result, the SWCNT nanoparticles comparatively gain maximum temperature than others. The increased thermal conductivity of the basefluid due to the use of nanoparticle of higher thermal conductivity increases the heat enhancement capacity of the basefluid.

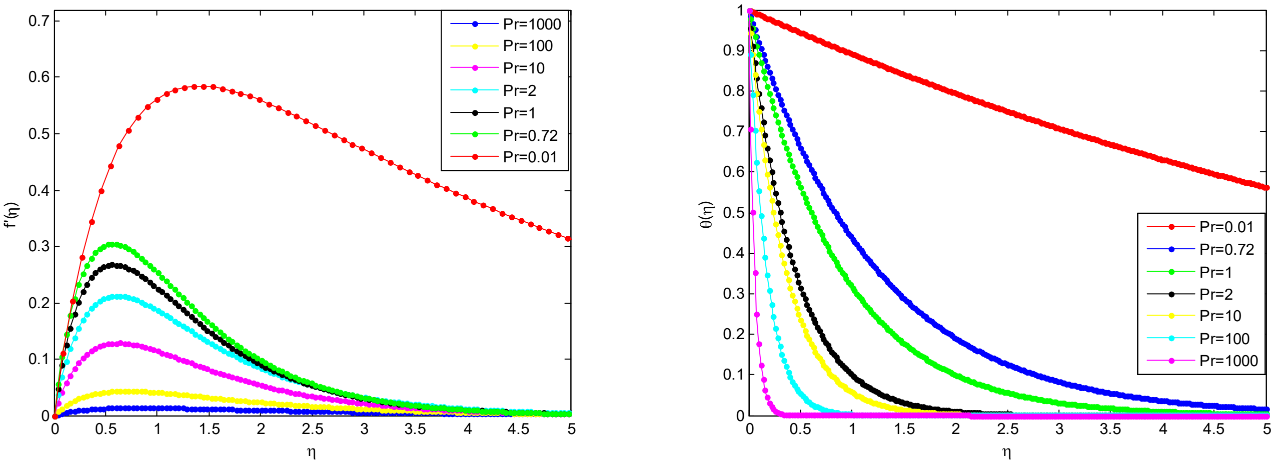

(a) velocity profile (b) temperature profile

Fig. 14. Effects of Prandtl number for TiO_2 nanoparticle

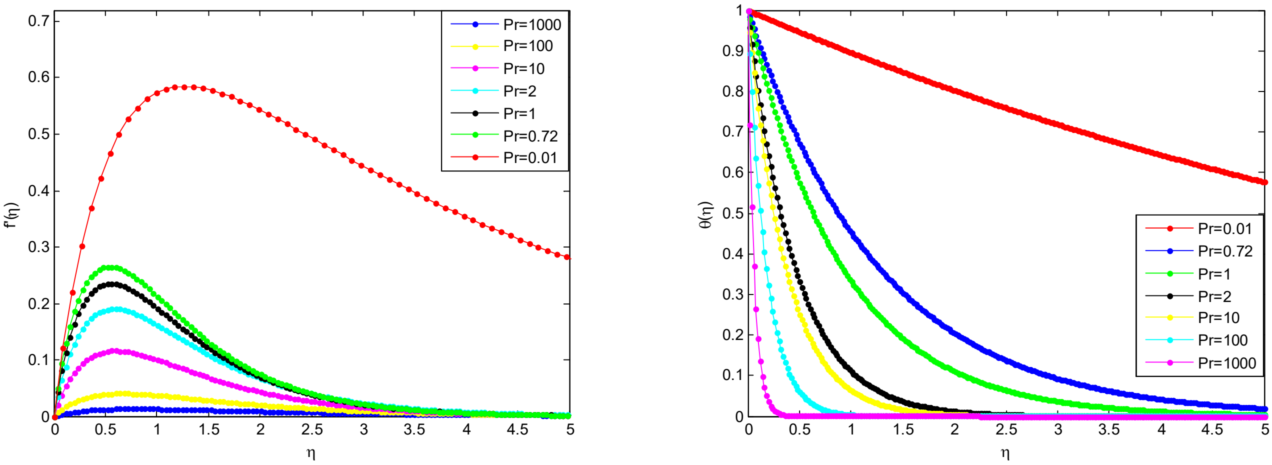

(a) velocity profile (b) temperature profile

Fig. 15. Effects of Prandtl number for CuO nanoparticle

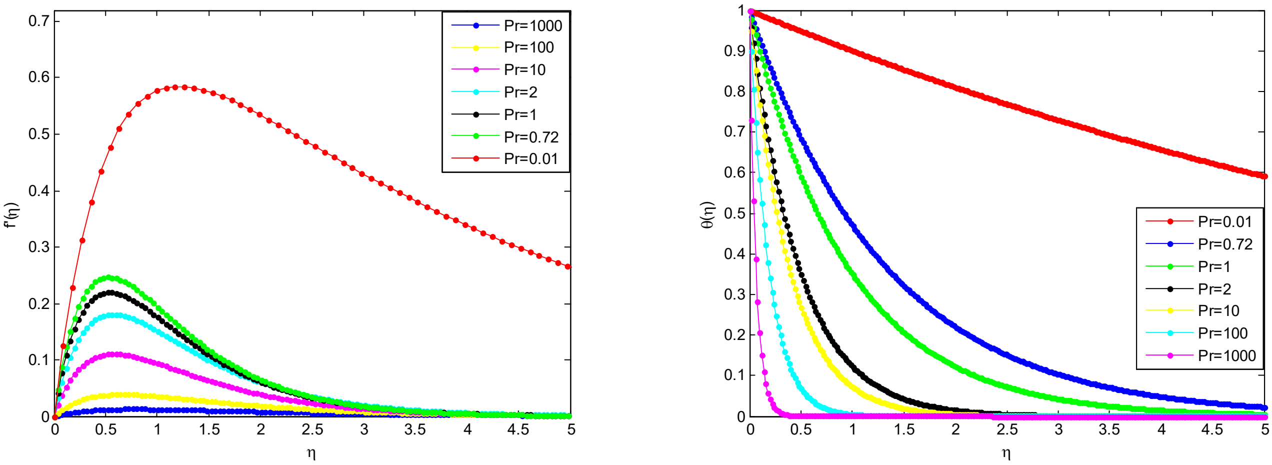

(a) velocity profile (b) temperature profile

Fig. 16. Effects of Prandtl number for Al_2O_3 nanoparticle

Also, it is observed that the decrease in velocity is maximum in SWCNT nanoparticles when compared with other type of nanoparticles. The reason is that the solid thermal conductivity has significant impacts on the momentum boundary layer of the nanofluid. The thickness of the momentum boundary layer increases by increasing the thermal conductivity. It is observed that the thickness of the thermal boundary layer enhances in presence of higher thermal conductivity nanoparticles. Therefore, the sensitivity of the boundary layer thickness to the type of nanoparticle is correlated to the value of the thermal conductivity of the nanoparticle used, which consequently leads to the enhancement of thermal conductivity of the nanofluid.

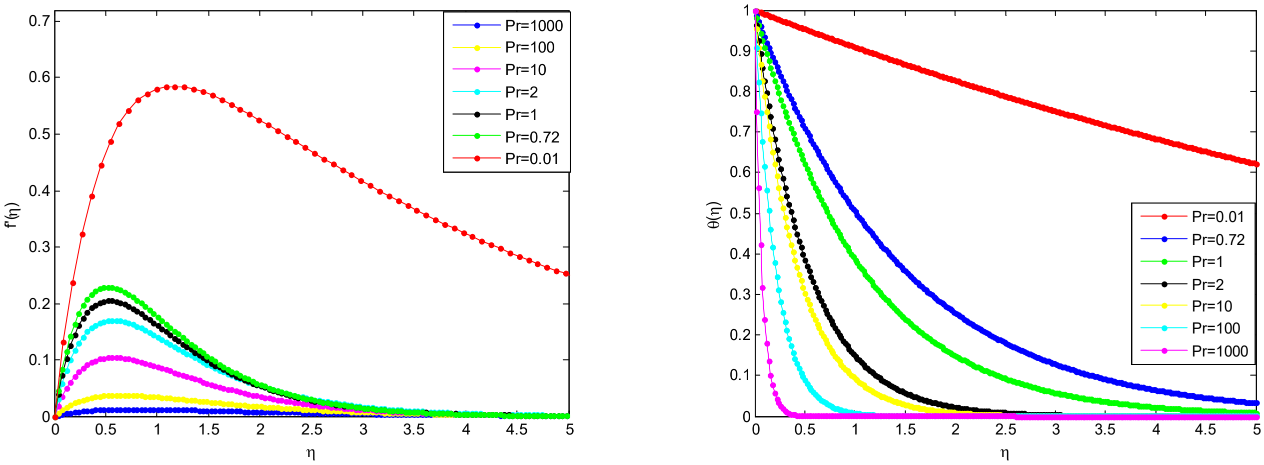

(a) velocity profile (b) temperature profile

Fig. 17. Effects of Prandtl number for SWCNTs nanoparticle

7. Conclusion

In this work, free convection boundary layer flow and heat transfer of nanofluids of differently- shaped nano-sized particles over a vertical plate at very low and high values of Prandtl number were analyzed. The governing systems of nonlinear partial differential equations of the flow and heat transfer processes were transformed to the system of nonlinear ordinary differential equation through similarity variables. The systems of fully coupled nonlinear ordinary differential equations was solved using differential transformation method- the Padé approximant technique. The accuracies of the developed analytical solutions were verified with the results generated by some other methods as presented in the past works. The developed analytical solutions were used to investigate the effects of the Prandtl number, nanoparticles' size and their shapes on the flow and heat transfer behavior of various nanofluids. From the parametric studies, the following observations were established.

i. The velocity of the nanofluid decreases as the Prandtl number increases but the temperature of the nanofluid increases as the Prandtl number increases.
ii. The velocity of the nanofluid decreases as the volume-fraction or concentration of the nanoparticle in the basefluid increases. However, an opposite trend or behavior in the temperature profile was observed, which showed that as the nanofluid temperature increases, the volume-fraction of the nanoparticles in the basefluid increases.
iii. The lamina shaped nanoparticle carries maximum velocity whereas the spherical shaped nanoparticle has a better enhancement on heat transfer than other nanoparticle shapes. The maximum decrease in velocity and maximum increase in temperature are caused by lamina shaped nanoparticles, followed by platelets, cylinders, bricks and sphere shaped nanoparticles, respectively.
iv. Using a common basefluid for all the nanoparticle types considered in this work, it was observed that SWCNT nanoparticles carry maximum decrease in velocity but have a better enhancement on heat transfer than other nanoparticle shapes. Also, it was observed that the maximum decrease in velocity and maximum increase in temperature were caused by TiO2, followed by CuO, Al2O3 and SWCNT nanoparticles, respectively.

The parametric studies reveal and expose the predominant factors as they affect the boundary layer of free convection flow and heat transfer of nanofluids. Moreover, the high level of accuracy and versatility of differential transformation method- the Padé approximate technique, has been demonstrated. It is hoped that the present study will enhance the understanding as it provides physical insights into the free convection boundary-layer problems.

Conflict of Interest

The authors declare no conflict of interest.

Nomenclature

c_p	specific heat capacity	β	volumetric extension coefficients
k	thermal conductivity	ρ	density of the fluid
m	shape factor	μ	dynamic viscosity
P	pressure	η	similarity variable
Pr	Prandtl number	λ	sphericity

u	velocity component in x-direction	ϕ	volume fraction or concentration of the nanofluid
v	velocity component in z-direction	θ	Dimensionless temperature
y	axis perpendicular to plates	f	fluid
x	axis along the horizontal direction	s	solid
y	axis along the vertical direction	nf	nanofluid

References

[1] E. Schmidt and W. Beckmann. Das temperatur-und geschwindigkeitsfeld vor einer wärme abgebenden senkrecher platte bei natürelicher convention. *Tech. Mech. U. Themodynamik*, Bd. 1(10) (1930), 341-349; cont. Bd. 1(11) (1930), 391- 406.

[2] S. Ostrach, An analysis of laminar free-convection flow and heat transfer about a flat plate parallel to the direction of the generating body force, *NACA Report*, 1111, 1953.

[3]. E.M. Sparrow and J.L. Gregg, Laminar free convection from a vertical plate with uniform surface heat flux, *Trans. ASME.* 78 (1956) 435-440.

[4]. E.J. Lefevre, Laminar free convection from a vertical plane surface, 9th Intern. Congress on Applied Mechanics, Brussels, paper I, 168 (1956).

[5]. E.M. Sparrow and J.L. Gregg, Similar solutions for free convection from a nonisothermal vertical plate, *Trans. ASME.* 80 (1958) 379-386.

[6]. K. Stewartson and L.T. Jones, The heated vertical plate at high Prandtl number, *J. Aeronautical Sciences* 24 (1957) 379-380.

[7]. H.K. Kuiken, An asymptotic solution for large Prandtl number free convection, *J. Engng. Math.* 2 (1968) 355-371.

[8]. H.K. Kuiken, Free convection at low Prandtl numbers, *J. Fluid Mech.* 37 (1969) 785-798.

[9]. S. Eshghy, Free-convection layers at large Prandtl number, *J. Applied Math. Physics* 22 (1971) 275 -292.

[10]. S. Roy, High Prandtl number free convection for uniform surface heat flux, *J. Heat Transfer* 95 (1973) 124-126.

[11]. H.K. Kuiken and Z. Rotem, Asymptotic solution for the plume at very large and small Prandtl numbers, *J. Fluid Mech.* 45 (1971) 585-600.

[12] T.Y. Na, I.S. Habib, Solution of the natural convection problem by parameter differentiation, *Int. J. Heat Mass Transfer* 17 (1974) 457–459.

[13]. J.H. Merkin, A note on the similarity solutions for free convection on a vertical plate, *J. Engng. Math.* 19 (1985) 189-201.

[14] J.H. Merkin, I. Pop, Conjugate free convection on a vertical surface, *Int. J. Heat Mass Transfer* 39 (1996) 1527–1534.

[15] F. M. Ali, R. Nazar, and N. M. Arifin, Numerical investigation of free convective boundary layer in a viscous fluid, *The American Journal of Scientific Research* 5 (2009) 13-19.

[16] S. S. Motsa, S. Shateyi, and Z. Makukula, Homotopy analysis of free convection boundary layer flow with heat and mass transfer, *Chemical Engineering Communications* 198(6) (2011) 783-795.

[17] S. S. Motsa, Z. G. Makukula and S. Shateyi. Spectral Local Linearisation Approach for Natural Convection Boundary Layer Flow. *Mathematical Problems in Engineering* (2013) Article ID 765013, 7 pages.

[18] A.R. Ghotbi, H. Bararnia, G. Domairry, A. Barari, Investigation of a powerful analytical method into natural convection boundary layer flow, *Communications in Nonlinear Science and Numerical Simulation* 14(5) (2009) 2222-2228.

[19] S. Mosayebidorcheh, T. Mosayebidorcheh. Series solution of convective radiative conduction equation of the nonlinear fin with temperature dependent thermal conductivity. *International Journal of Heat and Mass Transfer* 55 (2012) 6589-6594.

[20] S. Mosayebidorcheh, M. Farzinpoor, D.D. Ganji. Transient thermal analysis of longitudinal fins with internal heat generation considering temperature-dependent properties and different fin profiles, *Energy Conversion and Management* 86 (2014) 365–370.

[21] M. Hatami a, S. Mosayebidorcheh, D. Jing, Thermal performance evaluation of alumina-water nanofluid in an inclined direct absorption solar collector (IDASC) using numerical method, *Journal of Molecular Liquids* 231 (2017) 632–639.

[22] S. Mosayebidorcheh, Solution of the Boundary Layer Equation of the Power-Law Pseudoplastic Fluid Using Differential Transform Method, *Mathematical Problems in Engineering* (2013) Article ID 685454, 8 pages.

[23] S. Mosayebidorcheh, M. Hatami, D.D. Ganji, T. Mosayebidorcheh, S.M. Mirmohammadsadeghi. Investigation of Transient MHD Couette flow and Heat Transfer of Dusty Fluid with Temperature-Dependent properties, *Journal of Applied Fluid Mechanics*, 8(4) (2015) 921-929.

[24] S. Mosayebidorcheh. Analytical Investigation of the Micropolar Flow through a Porous Channel with Changing Walls, *Journal of Molecular Liquids* 196 (2014) 113-119.

[25] M. Sheikholeslami, S.A. Shehzad. CVFEM for influence of external magnetic source on Fe3O4-H2O nanofluid behavior in a permeable cavity considering shape effect, *International Journal of Heat and Mass Transfer* 115(A) (2017) 180-191

[26] M. Sheikholeslami, S.A. Shehzad. Magnetohydrodynamic nanofluid convective flow in a porous enclosure by means of LBM. *International Journal of Heat and Mass Transfer*, 113 (2017) 796-805

[27] M. Sheikholeslami, M. Seyednezhad. Nanofluid heat transfer in a permeable enclosure in presence of variable magnetic field by means of CVFEM. *International Journal of Heat and Mass Transfer* 114 (2017) 1169-1180

[28] M. Sheikholeslami, H.B. Rokni. Simulation of nanofluid heat transfer in presence of magnetic field: A review. *International Journal of Heat and Mass Transfer* 115(B) (2017) 1203-1233

[29] M. Sheikholeslami, T. Hayat, A. Alsaedi. On simulation of nanofluid radiation and natural convection in an enclosure with elliptical cylinders. *International Journal of Heat and Mass Transfer* 115(A) (2017) 981-991

[30] M. Sheikholeslami, Houman B. Rokni. Melting heat transfer influence on nanofluid flow inside a cavity in existence of magnetic field. *International Journal of Heat and Mass Transfer* 114 (2017) 517-526
[31] M. Sheikholeslami, M.K. Sadoughi. Simulation of CuO-water nanofluid heat transfer enhancement in presence of melting surface. *International Journal of Heat and Mass Transfer* 116 (2018) 909-919
[32] M. Sheikholeslami, Mohammadkazem Sadoughi. Mesoscopic method for MHD nanofluid flow inside a porous cavity considering various shapes of nanoparticles. *International Journal of Heat and Mass Transfer* 113 (2017) 106-114.
[33] M. Sheikholeslami, M.M. Bhatti. Forced convection of nanofluid in presence of constant magnetic field considering shape effects of nanoparticles. *International Journal of Heat and Mass Transfer* 111 (2017) 1039-1049.
[34] M. Sheikholeslami, M.M. Bhatti. Active method for nanofluid heat transfer enhancement by means of EHD. *International Journal of Heat and Mass Transfer* 109 (2017) 115-122.
[35] M. Sheikholeslami, Houman B. Rokni. Nanofluid two phase model analysis in existence of induced magnetic field. *International Journal of Heat and Mass Transfer* 107 (2017) 288-299.
[36] M. Sheikholeslami, S.A. Shehzad. Magnetohydrodynamic nanofluid convection in a porous enclosure considering heat flux boundary condition. *International Journal of Heat and Mass Transfer* 106 (2017) 1261-1269.
[37] M. Sheikholeslami, T. Hayat, A. Alsaedi. Numerical simulation of nanofluid forced convection heat transfer improvement in existence of magnetic field using lattice Boltzmann method. *International Journal of Heat and Mass Transfer* 108(B) (2017) 1870-1883.
[38] M. Sheikholeslami, T. Hayat, A. Alsaedi. Numerical study for external magnetic source influence on water based nanofluid convective heat transfer. *International Journal of Heat and Mass Transfer* 106 (2017) 745-755.
[39] M. Sheikholeslami, T. Hayat, A. Alsaedi, S. Abelman. Numerical analysis of EHD nanofluid force convective heat transfer considering electric field dependent viscosity. *International Journal of Heat and Mass Transfer* 108(B) (2017) 2558-2565.
[40] J.K. Zhou. *Differential Transformation and Its Applications for Electrical Circuits*. Huazhong University Press, Wuhan, China (1986) (in Chinese).
[41] L.T. Yu, C.K. Chen, The solution of the Blasius equation by the differential transformation method, *Math. Comput. Modell.* 28 (1998) 101–111.
[42] B.L. Kuo, Thermal boundary-layer problems in a semi-infinite flat plate by the differential transformation method, *Appl. Math. Comput.* 153 (2004) 143–160.
[43] B. L. Kuo. Application of the differential transformation method to the solutions of the free convection problem. *Applied Mathematics and Computation* 165 (2005) 63–79.
[44] M. M. Rashidi, N. Laraqi, S. M. Sadri, A Novel Analytical Solution of Mixed Convection about an Inclined Flat Plate Embedded in a Porous Medium Using the DTM-Pade. *International Journal of Thermal Sciences* 49 (2010), 2405-2412.
[45] N. S. Akbar and A. W. Butt. Ferro-magnetic effects for peristaltic flow of Cu-water nanofluid for different shapes of nano-size particles. *Appl. Nanosci.* 6 (2016) 379-385.
[46] M. Sheikholesmi, M. M. Bhatti. Free convection of nanofluid in the presence of constant magnetic field considering shape effects of nanoparticles. *International Journal of Heat and Mass Transfer* 111 (2017) 1039-1049.
[47] R. Ul Haq, S. Nadeem, Z.H. Khan, N.F.M. Noor. Convective heat transfer in MHD slip flow over a stretching surface in the presence of carbon nanotubes, *Physica B* 457 (2015) 40–47.
[48] L.D. Talley, G.L. Pickard, W.J. Emery, J.H. Swift. *Descriptive Physical Oceanography, Physical Properties of Sea Water*, sixth ed., Elsevier Ltd, 2011, 29–65.
[49] M. Pastoriza-Gallego, L. Lugo, J. Legido, M. Piñeiro. Thermal conductivity and viscosity measurements of ethylene glycol-based Al 2O3 nanofluids. *Nanoscale Res. Lett.* 6 (221) 1–11.
[50] S. Aberoumand, A. Jafarimoghaddam. Experimental study on synthesis, stability, thermal conductivity and viscosity of Cu–engine oil nanofluid, *Journal of the Taiwan Institute of Chemical Engineers* 71 (2017) 315–322.
[51] G.A. Baker, P. Graves-Morris. *Pade Approximants*, Cambridge U.P., 1996.
[52] H.K. Kuiken. On boundary layers in fluid mechanics that decay algebraically along stretches of wall that are not vanishingly small. *IMA Journal of Applied Mathematics* 27(4) (1981) 387–405.

Appendix A

The free convection boundary layer-type governing equations for the nanofluid flow are

$$\frac{\partial u}{\partial x}+\frac{\partial v}{\partial y}=0 \tag{A1}$$

$$\rho_{nf}\left(u\frac{\partial u}{\partial x}+v\frac{\partial u}{\partial y}\right)=\mu_{nf}\frac{\partial^2 u}{\partial y^2}+g\left(\rho\beta\right)_{nf}\left(T-T_\infty\right) \tag{A2}$$

$$\left(\rho C_p\right)_{nf}\left(u\frac{\partial T}{\partial x}+v\frac{\partial T}{\partial y}\right)=k_{nf}\frac{\partial^2 T}{\partial y^2} \tag{A3}$$

Introducing the stream function ψ and dimensionless temperature θ

$$u=\frac{\partial \psi}{\partial y}, \quad \mathrm{v}=-\frac{\partial \psi}{\partial x}, \quad \theta=\frac{T-T_{\infty}}{T_w-T_{\infty}} \tag{A4}$$

The continuity equation is satisfied and the momentum and energy equations become

$$\frac{\partial \psi}{\partial y}\frac{\partial^2 \psi}{\partial y \partial x}-\frac{\partial \psi}{\partial x}\frac{\partial^2 \psi}{\partial y^2}=\nu_{nf}\frac{\partial^3 \psi}{\partial y^3}+g\beta_{nf}\left(T_w-T_{\infty}\right)\theta \tag{A5}$$

$$\frac{\partial \psi}{\partial y}\frac{\partial \theta}{\partial x}-\frac{\partial \psi}{\partial x}\frac{\partial \theta}{\partial y}=\alpha_{nf}\frac{\partial^2 \theta}{\partial y^2} \tag{A6}$$

where

$$\nu_{nf}=\frac{\mu_{nf}}{\rho_{nf}} \quad and \quad \alpha_{nf}=\frac{k_{nf}}{\left(\rho c_p\right)_{nf}}$$

and the boundary conditions

$$\frac{\partial \psi}{\partial y}=\frac{\partial \psi}{\partial x}=0, \quad \theta=1 \text{ when } y=0 \tag{A7}$$

$$\frac{\partial \psi}{\partial y}=\frac{\partial \psi}{\partial x}=0, \ \theta=1 \text{ when } y=\infty \tag{A8}$$

The idea behind the similarity solution is that the velocity and temperature profile in different x in the boundary layer are geometrically similar, differing only by a stretching factor in the x-direction. Thus, the similarity variable should have the following form:

$$\eta=y\cdot m(x) \tag{A9}$$

where $m(x)$ is an unspecified stretching function. In order to reduce the partial differential equations (A5) and (A6) to ordinary differential equations, stream function ψ, which is a function of *x* and *y*, can be expressed as a function of *x* and η. If the similarity solution exists, one can expressed the stream function as

$$\psi(x,\eta)=\nu_{nf}f(\eta)\cdot s(x) \tag{A10}$$

where $f(\eta)$ and $s(x)$ are the similarity function and stretching function respectively. The dimensionless temperature can be assumed as a function of η only, i.e.

$$\theta(x,\eta)=\theta(\eta) \tag{A11}$$

From equations (A9) and (A10), one can develop the corresponding derivatives as

$$\frac{\partial \psi}{\partial y}=\nu_{nf}f'(\eta)\frac{\partial \eta}{\partial y}s(x)=\nu_{nf}f'(\eta)m(x)s(x) \tag{A12a}$$

$$\frac{\partial \psi}{\partial x}=\nu_{nf}f'(\eta)\,ym'(x)s(x)+\nu_{nf}f(\eta)s'(x) \tag{A12b}$$

$$\frac{\partial^2 \psi}{\partial y \partial x}=\nu_{nf}f'(\eta)\left[m'(x)s(x)+m(x)s'(x)\right]+\nu_{nf}f''(\eta)m'(x)s(x) \tag{A12c}$$

$$\frac{\partial^2 \psi}{\partial y^2}=\nu_{nf}f''(\eta)m^2(x)s(x) \tag{A12d}$$

$$\frac{\partial^3 \psi}{\partial y^3}=\nu_{nf}f'''(\eta)m^3(x)s(x) \tag{A12e}$$

$$\frac{\partial \theta}{\partial x}=\theta'(\eta)\frac{\partial \eta}{\partial y}=\theta'(\eta)\,ym'(x) \tag{A12f}$$

$$\frac{\partial \theta}{\partial y}=\theta'(\eta)\frac{\partial \eta}{\partial y}=\theta'(\eta)m(x) \tag{A12g}$$

where the prime for *f* and θ denote the derivatives with respect to η, while that of *s* and *m* denote with respect to *x*. Substituting the above derivatives into equations (A5) and (A6) and considering equation (A9), one obtains:

$$\begin{gathered}\frac{1}{(1-\phi)^{2.5}}f'''+\left[(1-\phi)+\phi\left[(\rho\beta)_s/(\rho\beta)_f\right]\right]\frac{g(\rho\beta)_f\left(T_w-T_{\infty}\right)}{\mu_{nf}^2m^3s}\theta \\ +\left[(1-\phi)+\phi\left(\frac{\rho_s}{\rho_f}\right)\right]\left\{\frac{s'}{m}ff''-\left[\frac{m's}{m^2}+\frac{s'}{m}\right](f')^2\right\}=0\end{gathered} \tag{A13}$$

$$\theta''+\left[\frac{1}{\left[(1-\phi)+\phi\left[(\rho C_p)_s/(\rho C_p)_f\right]\right]}\left[\frac{k_s+(m-1)k_f-(m-1)\phi\left(k_f-k_s\right)}{k_s+(m-1)k_f+\phi\left(k_f-k_s\right)}\right]\right]Pr\frac{s''}{m}f\theta'=0 \tag{A14}$$

In order to convert equations (A13) and (A14) to ordinary differential equations with η as the sole independent variable, all functions of x must be cancelled, which is possible only if the following combination of m and s and their derivatives are satisfied:

$$m^3 s = A = const \tag{A15}$$

$$\frac{s'}{m} = B = const \tag{A16}$$

$$\frac{m's}{m^2} = C = const \tag{A17}$$

Differentiation of equation (A15) and simplification of the resultant equation yields;

$$\frac{3m's}{m^2} + \frac{s'}{m} = 0 \tag{A18}$$

which is satisfied if equations (A16) and (A17) are satisfied. On substituting equation (A18) into (A13), one obtains

$$\begin{gathered}\frac{1}{(1-\phi)^{2.5}} f''' + \left[(1-\phi) + \phi\left[(\rho\beta)_s/(\rho\beta)_f\right]\right]\frac{g(\rho\beta)_f (T_w - T_\infty)}{\mu_{nf}^2 m^3 s}\theta \\ + \left[(1-\phi) + \phi\left(\frac{\rho_s}{\rho_f}\right)\right]\left\{\frac{s'}{m} ff'' - \frac{2}{3}\frac{s'}{m}(f')^2\right\} = 0\end{gathered} \tag{A19}$$

Therefore, satisfaction of equations (A15) and (A16) is sufficient to ensure that equations (A13) and (A14) become ordinary differential equations. Although any constant A and B in equations (A15) and (A16) will transform equations (A19) and (A14) into ordinary differential equations, the proper choice of values of these two constants will yield ordinary differential equation with simple forms. Choosing

$$\frac{g\beta(T_w - T_\infty)}{v^2 m^3 s} = 1 \tag{A20}$$

$$\frac{s'}{m} = 3 \tag{A21}$$

The corresponding s and m functions then become:

$$s(x) = 4\left(\frac{1}{4}Gr_x\right)^{1/4} \tag{A22}$$

$$m(x) = \frac{1}{x}\left(\frac{1}{4}Gr_x\right)^{1/4} \tag{A23}$$

where Gr_x is the local Grashof number defined as:

$$Gr_x = \frac{g\beta(T_w - T_\infty)x^3}{v^3} \tag{A24}$$

which is equivalent to the Reynolds number based on the scale of the local velocity $u_0 = \sqrt{g\beta_f(T_w - T_\infty)x}$. Substituting equation (A20) and (A21) into equation (A19) and (A14), the momentum and the energy equations become:

$$f''' + (1-\phi)^{2.5}\left\{\left[(1-\phi) + \phi\left(\frac{\rho_s}{\rho_f}\right)\right]\left(3ff'' - 2(f')^2\right) + \left[(1-\phi) + \phi\left[(\rho\beta)_s/(\rho\beta)_f\right]\right]\theta\right\} = 0 \tag{A25}$$

$$\theta'' + 3\left[\frac{1}{\left[(1-\phi) + \phi\left[(\rho C_p)_s/(\rho C_p)_f\right]\right]}\left[\frac{k_s + (m-1)k_f - (m-1)\phi(k_f - k_s)}{k_s + (m-1)k_f + \phi(k_f - k_s)}\right]\right] Prf\theta' = 0 \tag{A26}$$

which are obtained from Eqs. (A9), (A10), (A22) and (A23). Substituting the above expressions into Eqs. (A7) and (A8), the boundary conditions for Eq. (A25) and (A26) can be obtained as follows

$$f(\eta) = f'(\eta) = 0 \quad \text{and} \quad \theta(\eta) = 1 \text{ at } \eta = 0 \tag{A27}$$

$$f'(\eta) = \theta(\eta) = 0 \text{ at } \eta \to \infty \tag{A28}$$

It should be noted that for a viscous fluid which does not have nanoparticles, the nanoparticle volume fraction, $\phi=0$ and then one recovers from Eqs. (A25) and (A26) the earlier models of Ostrach [2] which was also used by Kuiken [7, 8, and 11].

$$f''' + 3ff'' - 2(f')^2 + \theta = 0 \tag{A29}$$

$$\theta'' + 3Prf\theta' = 0 \tag{A30}$$

and the boundary conditions remain the same as in Eq. (A28). The velocity components in the x and y directions can be expressed in terms of similarity variables by the following equations:

$$u=\frac{\partial \psi}{\partial y}=\frac{\partial \psi}{\partial \eta}\frac{\partial \eta}{\partial y}=\frac{2\nu_{nf}}{x}Gr_x^{1/2}f'(\eta) \tag{A31}$$

$$\mathrm{v}=-\frac{\partial \psi}{\partial x}=-\frac{\partial \psi}{\partial \eta}\frac{\partial \eta}{\partial x}=\frac{\nu_{nf}}{x}\left(\frac{1}{4}Gr_x\right)^{1/4}\left[\eta f'(\eta)-3f(\eta)x^{1/4}\right] \tag{A32}$$

Equations (A26) and (A27) are coupled non-linear ordinary differential equations with boundary conditions specified at different and they thus make the external natural convection a boundary value problem.